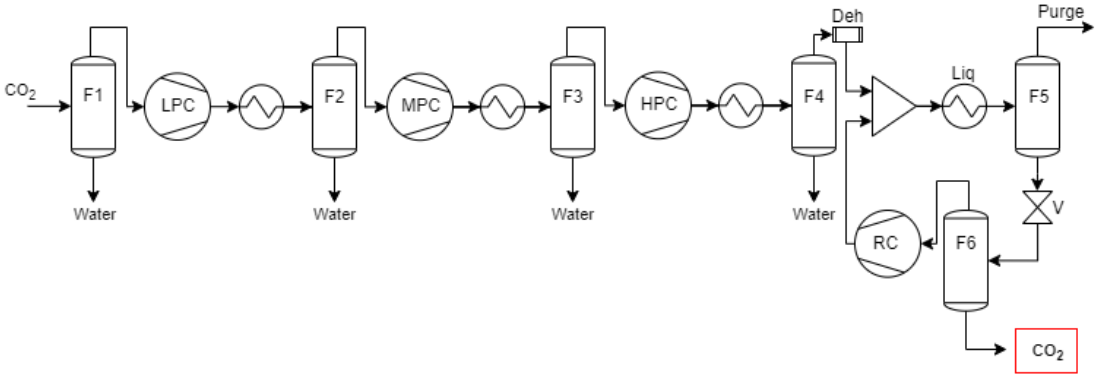

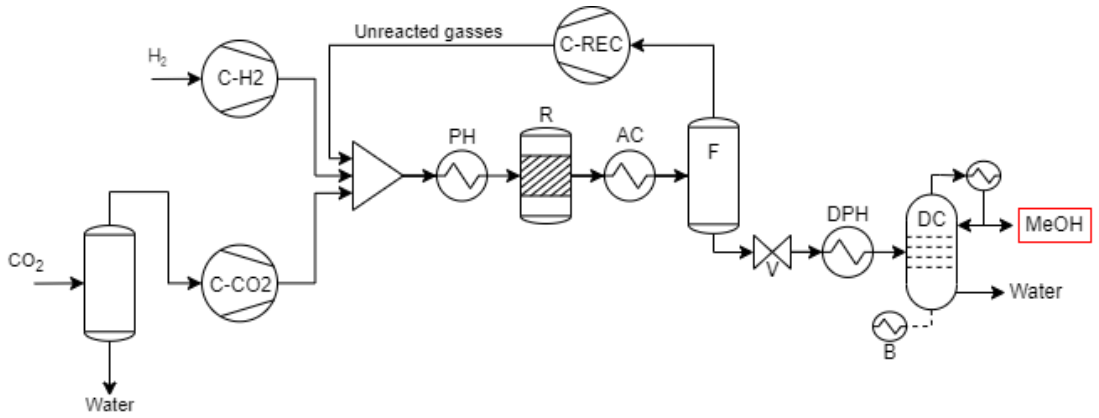

Assessment of Carbon Capture, Utilization and Storage for Gasendal

A techno-economic analysis for the pre-feasibility study of CCUS for a biogas upgrading plant

Master's thesis in Innovative Sustainable Energy Engineering, Heat and Power study track

SERGIO SAGASTUY BREÑA

DEPARTMENT OF MECHANICS AND MARITIME SCIENCE

CHALMERS UNIVERSITY OF TECHNOLOGY

Gothenburg, Sweden 2023

www.chalmers.se

Master's thesis 2023

Assessment of Carbon Capture, Utilization and Storage for Gasendal

A techno-economic analysis for the pre-feasibility study of CCUS for a biogas upgrading plant

SERGIO SAGASTUY BREÑA

CHALMERS
UNIVERSITY OF TECHNOLOGY

Department of Mechanics and Maritime Science
Division of Maritime Studies
Unit of Maritime Environmental Sciences
Chalmers University of Technology
Gothenburg, Sweden 2023

Assessment of Carbon Capture, Utilization and Storage for Gasendal
A techno-economic analysis for the pre-feasibility study of CCUS for a biogas upgrading plant
SERGIO SAGASTUY BREÑA

Industry Supervisor: Mariliis Lehtveer, Göteborg Energi AB
Academic Supervisors: Maria Grahn, Department of Mechanics and Maritime Sciences, and Mika Järvinen, Aalto University
Examiner: Maria Grahn, Department of Mechanics and Maritime Sciences

Master's Thesis 2023
Department of Mechanics and Maritime Science
Division of Maritime Studies
Unit of Maritime Environmental Sciences
Chalmers University of Technology
SE-412 96 Gothenburg
Telephone +46 31 772 1000

Cover: Schematics of the liquefaction (above) and e-methanol (below) processes proposed and studied

Typeset in LaTeX
Printed by Chalmers Reproservice
Gothenburg, Sweden 2023

Assessment of Carbon Capture, Utilization and Storage for Gasendal
A techno-economic analysis for the pre-feasibility study of CCUS for a biogas upgrading plant
SERGIO SAGASTUY BREÑA
Department of Mechanics and Maritime Science
Chalmers University of Technology

Abstract

In order to meet the goals set in the Paris Agreement and the stringent CO_2 emission level targets set in Sweden, there is an urgent need to increase the amount of CO_2 utilization and storage.

This thesis presents a techno-economic analysis of CO_2 liquefaction and the synthesis of electro-methanol (e-MeOH) as a CO_2 utilization pathway for captured CO_2 from Gasendal, a biogas upgrading plant. The processes are implemented and simulated in Aspen Plus to extract important parameters and calculate capital and operational costs as key performance indicators.

The results show that liquefaction costs 34 €/tonCO_2 for Gasendal, which is approximately 80% higher than shown in other studies. However, when increasing the plant size to 1M tonCO_2/year, the cost decreases to 10 €/tonCO_2. In terms of heat recovery potential, the plant could only provide heat to district heating, but the amount is too small considering no close pipelines.

On the other hand, e-methanol synthesis costs amounted to 1387 €/tonMeOH, with about 91% of expenses attributed to alkaline water electrolysis for hydrogen generation. Given that electrolysis costs pose a limitation and do not decrease with the scale of the plant in this study, the overall cost of e-methanol synthesis remains unaffected by the plant's capacity. Regarding heat recovery, the process is able to supply 98% of its heating demand and reduce the natural gas consumption in the existing process at Gasendal by around 43%.

Keywords: Carbon capture, carbon utilization, liquefaction, electrofuels, negative emissions.

Acknowledgements

Firstly, I would like to express my gratitude to my academic examiner, Maria Grahn, and my company supervisor from Göteborg Energi, Mariliis Lehtveer, for your constant support and guidance during our weekly meetings. I appreciate your willingness to allow me the flexibility to shape this thesis on my own. I am also thankful to everyone at the Energy Technology Division at Chalmers for their valuable time and assistance throughout this project. I would also like to acknowledge my second academic supervisor from Aalto University, Mika Järvinen, who consistently displayed a genuine interest in every idea put forth by students.

I'm extremely grateful to the family I made in Finland for teaching me that life is not solely about studying. Heartfelt gratitude goes to Julia, who provided unwavering support during the most challenging moments throughout my master's journey. I would also like to recognize the support from all the friends I made in Sweden, including classmates and office mates who not only supported me during stressful times but also encouraged me to simply have fun. My deepest gratitude goes to Gustavo, *gracias por acompañarme estos dos años y por siempre mostrarme todo lo que podía lograr.*

I could have not undertaken this two-year journey without the long-distance support from family members and friends. *Mamá y papá, gracias por siempre creer en mi y apoyarme en cada decisión que he tomado.* Many thanks to my brother and sister, *Javier y Mon, nunca me hubiera atrevido a tomar la decisión de venir a los países Nórdicos sin usar su valentía como ejemplo.* My deepest appreciation also goes to my aunt, *Amó, gracias por siempre ser mi seguidora número uno.*

Acknowledgments should also be extended to my friends from back home, who played a pivotal role in shaping my journey and influencing my decision to embark on this path. This includes my high-school friends, the "Pitzer" group from university, and my chosen second family, the Rancaño family.

Sergio Sagastuy Breña, Gothenburg, June 2023

List of Acronyms

Below is the list of acronyms that have been employed in this thesis:

ANP	Annualized Net Profit
AWE	Alkaline Water Electrolysis
BECCS	Bioenergy with Carbon Capture and Storage
CAPEX	Capital expenditure
CCS	Carbon Capture and Storage
CCU	Carbon Capture and Utilization
CCUS	Carbon Capture, Utilization and Storage
CEPCI	Chemical Engineering Plant Cost Index
CHP	Combined Heat and Power
CZA	Cu, ZnO and Al_2O_3 catalyst
DACCS	Direct Air Carbon Capture and Storage
DH	District Heating
e-fuels	Electro-fuels
e-MeOH	Electro-methanol
EOR	Enhanced Oil Recovery
GCC	Grand Composite Curve
HEN	Heat Exchanger Network
HEX	Heat Exchanger
HHV	Higher Heating Value
HP	High Pressure
ISBL	Inside Battery Limits
KPIs	Key Performance Indicators
LMTD	Logarithmic Mean Temperature Difference
LNG	Liquid Natural Gas
LP	Low Pressure
LPG	Liquid Propane Gas
MeOH	Methanol
MER	Maximum Energy Recovery
MP	Medium Pressure
NETs	Negative Emission Technologies
OPEX	Operational expense
PEMEL	Polymer Electrolyte Membrane Electrolysis
PR	Pressure Ratio

RB	Reboiler
RWGS	Reverse Water-Gas-Shift
SOEL	Solid Oxide Electrolysis
TAC	Total Annual Cost
TRL	Technology Readiness Level

Nomenclature

Below is the nomenclature for the parameters and variables that have been used throughout this project:

A	Heat exchanger area
C_e	Equipment purchased cost
C_{FC}	Total cost for fixed capital or total investment cost
D_i	Internal diameter of a column
E	Welding efficiency
H	Column height
m_t	Total mass flow rate
m_{CO_2}	CO_2 mass flow rate
m_{H_2}	H_2 mass flow rate
P_D	Distillation pressure
P_{del}	CO_2 delivery pressure
P_i	Initial pressure for the modeling/Internal pressure for vessel sizing
P_{liq}	CO_2 liquefaction pressure
P_R	Reaction pressure
Q	Heat duty
S	Maximum stress for vessel sizing/Equipment size for equipment cost estimation
T_{AC}	After-cooler temperature
T_{cool}	CO_2 compression inter-cooling temperature
T_D	Distillation temperature
T_{del}	CO_2 delivery temperature
T_i	Initial temperature
T_{liq}	CO_2 liquefaction temperature
T_R	Reactor temperature
U	Global heat transfer coefficient
x_{H_2O}	Water mass fraction
$\eta_{electrolysis}$	Water electrolysis electricity to hydrogen efficiency (based on HHV)

Contents

List of Figures

List of Tables

1

Introduction

The long-term temperature goal, as defined in the Paris Agreement in 2015, refers to the objective to stay well below 2°C of temperature increase since pre-industrial times with efforts to stay below 1.5°C [11]. The twelve months leading to January 2023 showed an average global temperature increase of 1.2°C [12]. The drastic temperature increase highlights the urgent need for a major transformation in the industrial and energy sector. As shown in Figure 1.1 from the International Energy Agency (IEA), industry, transport, and the power generation industries account for the vast majority of emissions within the energy sector. With a rapid transition to renewable energy, emissions from electricity generation can be reduced and part of the transport sector is projected to be rapidly electrified. Nonetheless, transport remains one of the areas that are hardest to decarbonize [13].

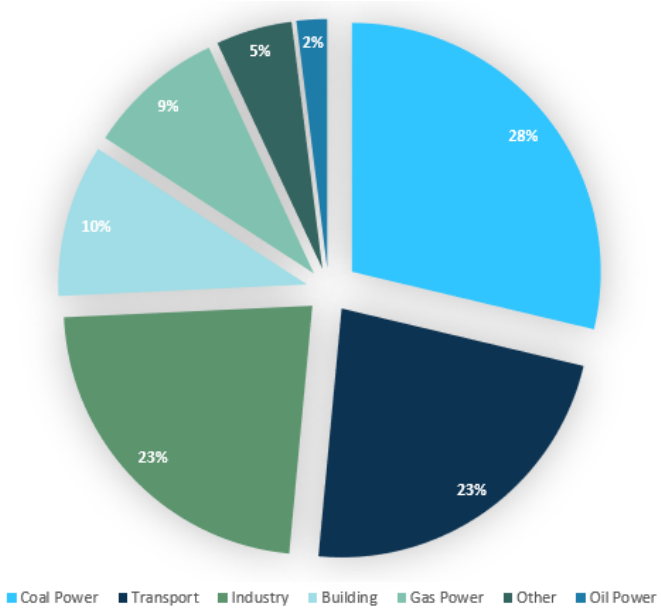

Figure 1.1: Energy sector share of CO_2 emissions (data extracted from the IEA [1])

Electrification of the transport sector is crucial to reduce greenhouse gas emissions and help mitigate climate change effects. Nonetheless, complete electrification may be unfeasible or unlikely, especially for long-distance travel or heavy-duty vehicles. Alternative options, such as biofuels and electrofuels (e-fuels), are necessary to reduce emissions in the transport sector. Gasendal, a biogas upgrading plant in the city of Gothenburg, shown in more detail in Section 3.1, provides biogas to the

natural gas network mainly for transportation purposes [14]. E-fuels involve the utilization of captured carbon dioxide (CO_2) combined with hydrogen (H_2) from water electrolysis to produce synthetic fuels. This possibility, together with CO_2 capture, is an example of Carbon Capture and Utilization (CCU). A few e-fuel synthesis pathways are explored in Section 3.3. Biogenic CO_2 emissions from Gasendal could serve as feedstock to synthesize e-fuels. This means that the plant could supply both biogas and e-fuels for the transportation sector.

Other pathways to tackle the reduction of CO_2 emissions include Carbon Capture and Storage (CCS), where the aim is storing CO_2 permanently or for a very long period of time. A combination of storage and utilization results in Carbon Capture, Utilization, and Storage (CCUS). This will be discussed more in-depth in Chapter 3, besides including an overview of Gasendal's process and facility, a primary motivation for this project, as well as a simplified schematic of the pathways available for captured CO_2. Societal and ethical challenges related to this work will also be discussed.

2
Aim

This thesis aims to evaluate the technical and economical feasibility of incorporating the synthesis of e-methanol (e-MeOH) as a way to utilize emissions of biogenic CO_2 from Gasendal, a biogas upgrading plant. Additionally, a second path including the upgrading, liquefaction, and sale of CO_2 to interested industrial sectors is considered, with a focus on liquefaction. The level of upgrading depends on the sector interested, so a review of CO_2 purity requirements is made. Heat integration potential is assessed, addressing the potential to recover heat for district heating as well. Based on predictions for future energy markets in Sweden, the feasibility of the projects is analyzed over time. The results will be compared with current costs for CO_2 conditioning. Future negative emission incentives including a possible price on negative CO_2 are further discussed given the results obtained. Gasendal's emission level of below 10,000 tons of CO_2 per year (see Table 3.1) makes the feasibility of e-fuel projects complicated to achieve as the upgrading plant is a small emitter. An impact on a higher level of emissions will be assessed, both for e-MeOH and the liquefaction process. It is expected that Gasendal should work as an excellent pilot project for future investments. On the other hand, a low level of emissions might be an advantage when considering sectors with lower CO_2 demand for their process.

2.1 Research questions

1. How does the feasibility of incorporating e-methanol production into Gasendal compare with other options such as CO_2 liquefaction for the sale of high-quality liquid CO_2 or CO_2 storage?
2. How should the liquefaction and utilization plants be designed in order to recover as much heat as possible?
3. How will future market conditions influence the feasibility of the projects?
4. What are the effects of up-scaling the processes? Are the projects scalable to other processes such as biomass-powered CHP plants?

2.2 Limitations

- The objective is not to perform a detailed simulation of the different processes, but rather to map several options and compare alternatives. Simulation software serves as a complementary tool to map the routes.
- The feasibility is based on key performance indicators (KPIs), such as CAPEX, OPEX, and annualized net profit without considering transportation to the

end-user or storage.
- The boundary conditions are within the two processes studied.
- The e-fuel option e-methanol is chosen as an example of a CO_2-derived product. Other e-fuel options include e-methane, e-gasoline, or e-jet-fuel, among others. This thesis disregards the assessment of the other options, where some face feasibility challenges at such a small scale and others are being assessed in parallel MSc. thesis work.
- Detailed reaction mechanisms and kinetics are not considered for the design of the utilization process plant.
- No optimization for hydrogen production is performed. A constant supply is assumed.
- The project is not based on analyzing adequate market conditions to make the alternatives feasible, but rather on assessing the profitability of the projects within the current market and making assumptions on future feasibility.

3
Background

3.1 Gasendal

Gasendal is Göteborg Energi's first biogas plant and upgrades gas from the regional wastewater treatment plant Ryaverket, owned by Gryaab. The biogas coming from the anaerobic digestion process at Ryaverket, which will be referred to as raw gas, is piped through two compressors to Gasendal's facility where the first step is a carbon filter to remove hydrogen sulfide (H_2S). This step is also important for the utilization of CO_2 in processes like power-to-gas, where the catalyst can be very sensitive to H_2S [15]. Roughly, the composition of the raw gas is 60% methane (CH_4) and about 40% CO_2, but contains water and small traces of H_2S [7].

After the carbon filter, the raw gas is transported to a conventional absorption separation unit to separate CH_4 from CO_2. An amine solution, which works as the absorbent, absorbs the CO_2 from the gas mixture. Consequently, concentrated CH_4 exits through the top of the absorber column. The CO_2-rich amine solution is pumped to the desorber, or stripper, where, on a heat-driven separation process, CO_2 is separated from the absorbent at a temperature of 105°C [7]. In order to recover the evaporated fraction of the amine solution, CO_2 is cooled down before being released into the atmosphere [15]. The energy provided to the stripper comes from steam generated in one of two available natural gas-fired boilers, as reported in the 2020 Environmental Report from Gasendal [7].

CH_4 is compressed, dried in an adsorption dryer, and a filter is used to control the quality of the biogas (99.7% purity). Propane is added in the final step, before sending the upgraded biogas to the natural gas network, in order to increase its heating value [7].

Table 3.1: Results from 2020 reported in the 2020 Environmental Report for Gasendal [7]

	Flow per year	Energy flow (GWh)
Raw gas inlet (kNm^3)[a]	10,246	62
Upgraded biogas (kNm^3)[a, b]	6,967	71
Propane consumed (ton)	318	
Total $CO_{2,eq}$[c](ton)	9,226	
Biogenic CO_2 (ton)	7,682	

[a] N refers to Normal Temperature and Pressure (NTP) conditions of 20°C and 1 atm
[b] Including added propane
[c] $CO_{2,eq}$ calculated based on the Global Warming Potential (GWP) of greenhouse gas emissions

3.2 Net zero emissions, negative emissions and the role of Carbon Capture, Utilization, and Storage

According to the objectives outlined in Sweden's climate policy framework, by 2045, the aim is to achieve zero net emissions of greenhouse gases, followed by attaining negative emissions thereafter [16]. Within this objective, CCS plays a significant role with particular relevance placed on Bioenergy with Carbon Capture and Storage (BECCS). BECCS, as it involves capturing and storing biogenic CO_2 results in a net removal of CO_2 from the atmosphere. BECCS, together with high levels of reforestation and afforestation, and Direct Air Carbon Capture and Storage (DACCS) are examples of Negative Emission Technologies (NETs). NETs are essential technologies in order to meet the climate goals set in the Paris Agreement [11].

Controversy often arises with the utilization of captured fossil CO_2 as it could be later emitted into the atmosphere, thus relocating, but not reducing CO_2 emissions. Utilization of biogenic CO_2, however, offers the possibility to displace the use of fossil fuels and maintain net zero emissions. Biogenic CCU or Bioenergy with Carbon Capture and Utilization (BECCU) then seem like promising alternatives in sectors difficult to decarbonize such as transport. In Gasendal, biogenic CO_2 is separated from the incoming raw biogas and various options are available for its subsequent use, including storage for achieving negative emissions or utilization. Utilization of the captured CO_2 could replace or reduce the combustion of fossil fuels and aid decarbonization in other sectors.

Within this project, BECCS and BECCU are not specifically addressed, since there is no energy conversion process involving the release of CO_2 due to combustion to produce heat and electricity. The process studied is better described as biogenic CCUS, otherwise known as bio-CCUS.

3.3 Captured carbon dioxide pathways

Several possible pathways for captured CO_2 are mapped in Figure 3.1. In order to reach negative emissions, CO_2 has to be stored permanently. Storage options include old oil and gas reservoirs, unminable coal beds, deep saline aquifers, and CO_2 mineralization [17]. Enhanced Oil Recovery (EOR) is also an option within geological storage solutions. The latter relies on using captured CO_2 to extract more oil from reservoirs while at the same time trapping most of the gas underground. Therefore, EOR works as both utilization and storage. Nonetheless, the storage is temporary as blowing down of the reservoir pressure results in a small but considerable quantity of CO_2 being released again into the atmosphere [18]. Moreover, EOR promotes the extraction of more fossil resources that would in turn result in additional anthropogenic CO_2 emissions. Since this project focuses on the utilization and storage of biogenic CO_2 to reach net zero and negative emissions, EOR is not considered a suitable option.

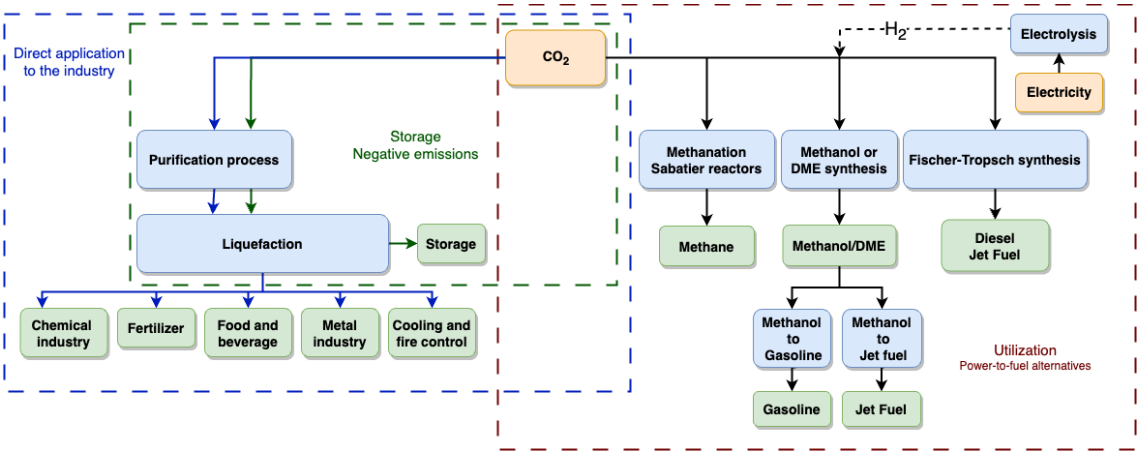

Figure 3.1: Pathways for utilization and storage of CO_2

The right side of Figure 3.1, encompassed by the red box, shows a summary of the utilization of CO_2 paths to synthesize e-fuels adapted from a review paper by Grahn et al. [19]. In this case, e-fuels are defined as fuels produced by combining recycled CO_2 and electrolytic hydrogen [20]. This term will make reference to all the different fuels that can be produced following the same principle, although the conversion technology varies. In principle, they all work as electricity storage liquids or gases [20] and the process can also be defined as power-to-liquid or power-to-gas [13].

Categorizing a fuel as carbon neutral does not only mean that its carbon source has to be biogenic, but also that renewable electricity has to power the fuel's synthesis process. This entices new problems related to the intermittency of renewable sources and the current energy system. Nonetheless, with decreasing running costs, renewable electricity has become the regular option for energy scenarios [13]. Likewise, hydrogen is an excellent electricity storage solution for high electricity generation with low demand [20]. The cost of solar and wind energy is so low that electricity is produced whenever available regardless of demand [13]. Hence, storage solutions

other than batteries and hydropower are imperative.

Research on renewable fuels has taken an interest over the last years as society and governments push toward major changes in the energy system. Biofuels and e-fuels have been researched as alternative options to substitute the use of fossil fuels and reach net zero emissions in the transport and industrial sector. Nonetheless, there are few studies on the application of such technologies in larger-scale plants. This thesis looks to aid Göteborg Energi and study the impact of implementing e-fuel production in Gasendal as a utilization path of captured CO_2. Agersborg and Lingehed [15] performed simulations to assess the feasibility of power-to-gas in Gasendal in 2013. This project intends to map alternative routes, such as e-MeOH with the aim of expanding the knowledge on the application of these technologies in biogenic carbon sources like Gasendal.

On the other hand, the area referred to as direct application to the industry, encompassed by a blue box in Figure 3.1, will also be explored. CO_2 can be purified and liquefied on-site, and sold to interested parties in sectors such as plastics, food and beverage, metal industry, for cooling and refrigeration purposes, amongst other options. A focus on the liquefaction process is made in this thesis since it is the common process for both the direct application of CO_2 and storage.

3.4 E-methanol

Methanol (MeOH) has the potential to be used as a fuel or as a precursor for other chemicals like dimethyl ether, formaldehyde, and acetic acid, amongst others. It also presents the lowest production cost-to-market price ratio when compared to other power-to-fuel alternatives [21]. Within the electrofuel options presented in Figure 3.1, the fuel to be explored in this project is e-MeOH, given its versatility to be used as an energy carrier itself or the possibility to convert it to other valuable fuels, such as gasoline or jet-fuel. Additionally, prior research conducted at Gasendal has explored the electro-methane synthesis, also known as power-to-gas [15], paving the way for investigating other integrated power-to-fuel alternatives, including e-MeOH.

Conventionally, MeOH comes from synthesis gas (syngas) produced from natural gas or other fossil resources [22]. Syngas is a mixture of gases, including carbon monoxide (CO), CO_2, H_2, and other species at lower concentrations. With the steam methane reforming process, pure syngas can be produced using catalysts based on copper (Cu) and zinc (Zn) since the 1960s [23]. Before that, other oxide catalysts were used and high pressure and temperature conditions were required [24]. Reactions 3.1-3.3 are involved in the synthesis of MeOH (having the chemical formula CH_3OH) [25].

$$CO_2 + 3H_2 \rightleftharpoons CH_3OH + H_2O \qquad \Delta H_{298K} = -49.51 kJ/mol \tag{3.1}$$

$$CO_2 + H_2 \rightleftharpoons CO + H_2O \qquad \Delta H_{298K} = 41.17 kJ/mol \tag{3.2}$$

$$CO + 2H_2 \rightleftharpoons CH_3OH \qquad \Delta H_{298K} = -90.68 kJ/mol \tag{3.3}$$

The Reaction 3.1 corresponds to the direct hydrogenation of CO_2 to MeOH. Reaction 3.2 is the reverse water-gas shift reaction (RWGS) and Reaction 3.3 is the hydrogenation of CO. The essential reaction for conventional MeOH is the hydrogenation of CO, which is exothermic as shown above [24]. Nonetheless, the other two reactions are also expected because of the presence of CO_2 in syngas.

The synthesis of e-MeOH, known as power-to-methanol, comes as an alternative, cleaner option than traditional MeOH synthesis. This pathway involves the direct hydrogenation of CO_2 to MeOH using H_2 from water electrolysis powered by renewable electricity, offering the possibility to utilize captured CO_2. The predominant reaction now becomes the hydrogenation of CO_2 (Equation 3.1) [24]. Both the hydrogenation of CO and CO_2 are exothermic, as can be seen in the reaction enthalpy, although the amount of energy released by converting CO_2 to MeOH is less than using CO as a feed-stock. The RWGS reaction occurs at the same time, but it is endothermic [24]. Since CO is produced with the RWGS reaction it is expected that the hydrogenation of CO will also be present when producing MeOH from CO_2, but it can be considered as a secondary reaction.

Given the reactions above, for CO_2 hydrogenation, higher pressures favor the reaction since there is a reduction in the number of moles. Also, exothermic reactions are favored at lower temperatures, which is why the yield decreases at higher temperature levels [24]. However, faster reaction kinetics can be expected at higher temperatures.

MeOH coming directly from CO_2 has certain advantages over the traditional process, given that the production results in fewer by-products, requiring less energy for purification [26]. Having a purer reactant source, the reaction chemistry is also simplified [22]. However, the cost of e-methanol is 2 to 2.5 times higher than conventional methanol synthesis methods [21, 26].

3.4.1 Water electrolysis

Water electrolysis is the process of splitting water molecules through a potential difference between two electrodes in an electrolyte [27]. The main electrolysis technologies are alkaline water electrolysis (AWE), polymer electrolyte membrane electrolysis (PEMEL), and solid oxide electrolysis (SOEL) [19]. SOEL is still under development [28] and won't be considered as a possibility in this thesis. PEMEL uses a solid polymer as the electrode and also as the membrane [27]. PEMEL is a commercialized technology [28], so the technology readiness level (TRL) can be assumed to be between 8 to 9. TRL level of 9 is the highest which means that the technology is already commercialized and competitive. AWE is also commercialized and it is the most mature technology [29]. This technology uses an alkaline solution as the electrolyte, which is commonly potassium hydroxide (KOH). Nickel is used as an electrode in AWE, so no expensive metals are required [30]. AWE operates

at temperatures that range between 70 to 90°C and a maximum pressure of 30 bar [29, 31].

3.4.2 Catalyst and reaction kinetics

Although the catalyst is not investigated in this project, it is noteworthy to say that CO_2 hydrogenation is a catalytic process. The catalyst employed in the industry is based on Cu, ZnO, and Al_2O_3, which is commonly referred to as CZA [24]. This catalyst is more efficient when there's a mixture of CO and CO_2, but it is still the one that is used the most because it is a well-established catalyst option [32]. The kinetic model by Graaf et al. [33–35], based on a commercial CZA catalyst is the prevailing choice for calculating and estimating reaction kinetics in MeOH synthesis.

Seidel et al. [36] present an alternative model, owing to the fact that the mechanism from Graaf et al. considers only one type of active center in the catalyst. Seidel et al. [36] take into account different active centers presenting a more accurate kinetic model. Torcida et al. [37] present a reactor design for multi-bed reactors for the direct hydrogenation of CO_2 with CZA as a catalyst following a Langmuir-Hinshelwood model presented by Seidel et al. [36]. The Langmuir-Hinshelwood model refers to the reaction mechanism presented by Langmuir and Hinshelwood [38].

3.5 Liquefaction of carbon dioxide

Liquefaction requires a series of compression and/or cooling stages. To decide the liquefaction technique and parameters, it is important to define the delivery pressure (P_{del}) and temperature (T_{del}). In conventional liquefied propane gas (LPG) and liquefied natural gas (LNG) transport, liquid conditions are maintained with refrigeration and atmospheric pressure [39]. Figure 3.2 shows the phase diagram for CO_2 obtained using the diagram presented by Deng et al. who used the Span and Wagner equation of state [2]. It is shown here that at atmospheric pressure, CO_2 only exists as a gas or solid. Therefore, pressurization is required to ensure liquid conditions for transport and storage. Low pressures are favorable for safe transport.

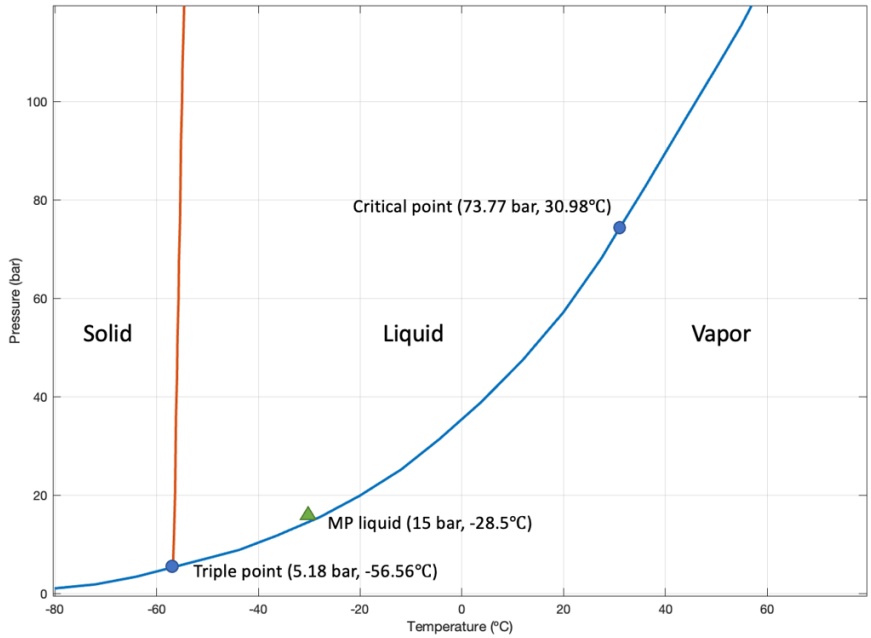

Figure 3.2: CO_2 phase diagram traced from approximating the data presented in the diagram from [2]

.

For the direct application of CO_2 in the industry, and storage, CO_2 has to be transported to the end-user, storage site, or intermediate storage facility. CO_2 can be transported in different conditions and different phases, including gas, liquid, supercritical conditions, and even solid as dry ice. Compressed gas transport in pipelines is a possibility, but generally, pipe transport will be considered for larger quantities and shorter distances. Ship transport for longer distances and small volumes could be a better option than pipelines [2]. Ship transport requires CO_2 to be in the liquid phase since it is safer and requires a smaller volume than in the gas phase. Similarly, transport in trucks is beneficial for smaller volumes when compared to pipelines. Therefore, transport in tanks requires the CO_2 to be liquid at a low-pressure level [40]. The choice of transport conditions is discussed further in Section 3.5.1.

3.5.1 Delivery pressure of carbon dioxide

Delivery pressure is defined as the pressure at which the CO_2 leaves the liquefaction plant for storage or transport. Therefore, in this thesis, delivery conditions are considered the same as transport conditions. Transport pressure will be divided into three categories: low pressure (LP) at 6 barg (gauge pressure) and -50°C, medium pressure (MP) at 15 barg and -28°C and high pressure (HP) at 70 barg and 0°C. HP won't be considered since such high pressurized gas would require several small storage or transport tanks and would become too expensive [41].

An example of a project for the transport of CO_2 is CO2LOS, carried out by Brevik

Engineering AS and SINTEF [41]. The project presented a study on liquefaction pressures in their final report for phase II of the project [42]. LP CO_2 has a higher density and, since there is less stress on materials, it is possible to have larger tanks for transport with thinner plates. To control the temperature and pressure of the tank when unloading, 1.8% of the cargo has to be left in the tank. On the other hand, MP is a mature technology, operating with a safe margin from the triple point, which prevents the formation of dry ice. In this case, 4% of the cargo has to be left on the tank when unloading, which represents less efficient transport. In terms of costs, liquefaction to MP is cheaper because cooling is more expensive than compression [42].

For lower liquefaction costs, it would be preferable to compress CO_2 to the MP level which requires less cooling. Nonetheless, transport is cheaper and more efficient at lower pressure, although no ships are operating at these conditions yet [42]. MP transport for small quantities of food-grade CO_2 is a proven technology [2]. In Figure 3.2, the MP liquid point is shown, matching the exact conditions required by intermediate storage project CinfraCap [43]. It is possible to visualize the safe distance from the triple point. Furthermore, CO_2 in this condition is slightly subcooled, as shown in the diagram.

3.6 Societal and ethical challenges addressed

The transformation of the energy system to try, to the best of our abilities, to meet the climate goals and stay well below a 2°C temperature increase since pre-industrial times can have a major impact on society. The loss of jobs within the fossil energy sector is a concern. The implementation of renewable fuel production plants will create jobs that can address this issue. There is a major increase in job opportunities in the electricity sector with a switch to renewable power generation towards 2050 [44]. The same could be expected of the renewable fuel industry for transportation. This thesis, by providing more information on the feasibility of e-fuels, aims to aid the transition to renewable fuels which would in turn generate advanced job opportunities. Similarly, the evolution of biogenic carbon dioxide markets will require new infrastructure and new processing technologies, providing new opportunities and alternative options to the current fuel industry.

Alternatively, biofuels are one of the substitutes for fossil resources. However, there are concerns in terms of land use impacts that have incentivized a lot of research on sustainable biomass supply for biofuels. Similarly, food production is expected to increase taking a lot of land space, highlighting the importance of reducing the dependence on biomass for energy [13]. E-fuels are an alternative to decrease the demand for biofuels in the transport sector, for example. This would also allow for the focus of bio-energy on heat and electricity generation and the implementation of BECCS for must-needed negative emissions. Moreover, biomass combustion would also switch more anthropogenic emissions into biogenic CO_2. These emissions can consequently be used to produce more carbon-neutral e-fuels [13].

4

Methods and material

Firstly, a review of purity requirements and the direct application to the industry is performed to provide insight into the considerations that are required for future feasibility studies for Gasendal and other related processes. Then, the two chosen pathways for CO_2 (i.e. e-MeOH and liquefaction) are mapped based on basic designs of the processes to address the technical feasibility of the projects. The models are simulated to determine important process parameters that are needed to perform the techno-economic analysis. The first model constitutes the e-MeOH synthesis route. The second process simulated is the liquefaction of CO_2 up to transport temperature and pressure conditions. This model will serve as a basis for the direct application of CO_2 to interested industrial sectors, as well as when it is sent to storage. Potential sectors are considered for the sale of the product, but these are only mentioned, together with the CO_2 purity requirements. To reduce energy consumption and minimize cost, pinch analysis is performed to assess the heat recovery potential within the process, to reduce energy consumption at Gasendal, and to utilize heat for district heating (DH). The capital investment and operational costs are considered as key performance indicators (KPIs) of the different captured CO_2 pathways.

This section gives an overview of the methodology followed in this thesis. After describing the purity requirement review, a description of the chosen processes is presented. Secondly, the details on the generation of the digital twins in Aspen Plus are shown. The technical analysis methodology section ends with a description of the application of pinch analysis to both processes and equipment sizing methodology. The last part of this section describes the economic assessment.

4.1 Purity review

CO_2 coming from Gasendal is assumed to be pure with only water. However, this is seldom the case and the presence of impurities needs to be considered. Deng et al. [2] performed a study to assess the impact of impurities present in CO_2 before liquefaction. For the purpose of summarizing important information for future studies that focus on gas treatment and the presence of impurities, a review is performed regarding the possible presence of impurities, and the purity requirements by the industry are included. Additionally, a brief description of potential CO_2 applications is presented.

4.2 Technical analysis

Energy and mass balances are performed using Excel and MATLAB R2022B based on annual average energy and mass flows from Gasendal. Process modeling is performed on Aspen Plus V12.1 and CoolPack. Heat integration is assessed using pinch analysis with the Aspen Energy Analyzer software.

4.2.1 E-methanol process description

Based on reaction stoichiometry, it is possible to calculate and estimate reactant quantities, as it was done by Rufer et al. [25]. The authors assessed the feasibility of producing e-methanol from DACC by performing a quantitative analysis of the process. The required hydrogen was calculated taking into account reaction 3.1 for CO_2 hydrogenation presented in Section 3.4.

The process was designed according to that proposed by Meunier et al. [45] but simplified without including heat integration for the base case. This is because, although important temperature levels are set at the same level as the authors proposed, the heat content in the streams changes, resulting in a different heat exchanger network (HEN). The process block diagram is shown in Figure 4.1.

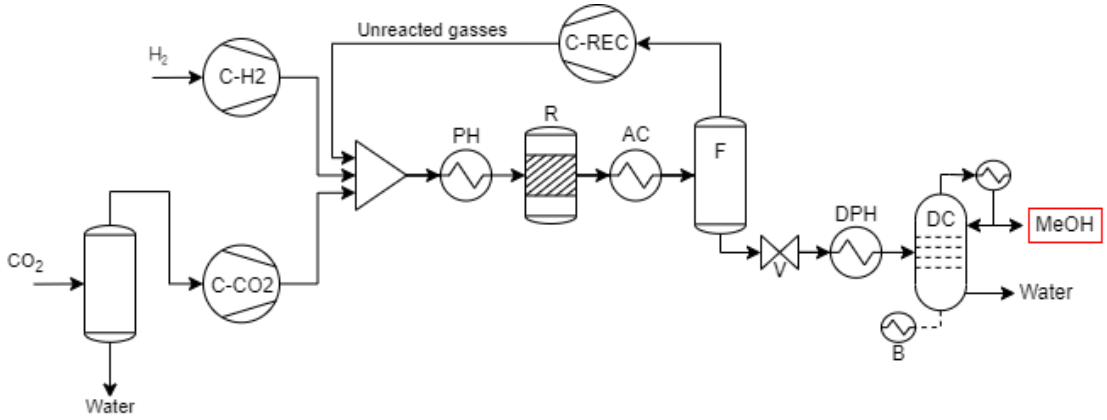

Figure 4.1: General schematics of the proposed e-methanol synthesis process

H_2 is compressed from 30 bar to the reaction pressure of 80 bar in a one-stage compressor (C-H2). On the other hand, CO_2 first goes through a knockout drum to ensure no liquid goes into the compressor. Then it goes into a 4-stage compressor train (C-CO2) with intercooling. This is designed as proposed by Meunier et al. [45], where heat is recovered to be used by the carbon capture reboiler unit by intercooling in between compressor stages to a temperature of 128°C. A compressor train of four stages was also proposed by Pérez-Fortes et al. [32], confirming that this is an adequate choice. CO_2 is compressed from 1 bar to 80 bar with an equal pressure ratio (PR) in the four stages (i.e. PR of 2.98). The reactants are then mixed with unreacted gases and go through a pre-heater (PH) to reach the reaction temperature of 250°C. The outlet stream of the reactor is then cooled in a cooler defined as

after-cooler (AC) to 40°C to condense the products (mainly MeOH and water) and separate un-reacted gases in a flash separator (F). These gases are recirculated to the reactor. The products are recovered from the bottom of flash tank (F) and expanded to 1 bar in the expansion valve (V) before being heated up to 90°C in the distillation pre-heater (DPH). The pre-heated stream goes into the distillation column (DC), where distillation is carried out with heat being provided by a boiler (B), and water is recovered at the bottom of the column at a temperature close to 100°C. At the top of the column, MeOH is recovered and condensed. The characteristics of the condenser and distillation reflux ratio are defined given the simulation results and this is explained in Section 4.2.3. A summary of the input data mentioned is shown in Table 4.1.

Table 4.1: Aspen Plus e-methanol synthesis input data for the base case

Parameters	ID	Value
CO_2 total inlet (kg/h)	m_{CO_2}	928
Water content at CO_2 inlet (wt%)	x_{H_2O}	2%
H_2 inlet (kg/h)	m_{H_2}	125.38
CO_2 inlet pressure (bar)	Pi_{CO_2}	1
H_2 inlet pressure (bar)	Pi_{H_2}	30
CO_2 inlet temperature (°C)	Ti_{CO_2}	23
H_2 inlet temperature (°C)	Ti_{H_2}	25
Reaction pressure (bar)	P_R	80
Reaction temperature (°C)	T_R	250
Aftercooling temperature (°C)	T_{AC}	40
Distillation inlet temperature (°C)	T_D	90
Distillation pressure (bar)	P_D	1

For the production of H_2, AWE is chosen as it is the most mature technology. The pressure of electrolysis is set to 30 bar, to reduce the compression work in the synthesis of e-MeOH. Thus, the inlet of H_2 to the process is at 30 bar. AWE operates at a temperature of about 70 °C, but an assumption was made that heat is recovered in the electrolysis process. Therefore, H_2 is supplied to the methanol plant at 25°C. Nonetheless, heat integration for electrolysis goes beyond the scope of this thesis.

4.2.2 Liquefaction process description

There are two options to design a liquefaction process. The first one is high-pressure compression and then CO_2 is liquefied by expansion [3]. This is also known as open-cycle liquefaction [40]. The second and cheaper option is low-pressure liquefaction, where the gas is first compressed and then liquefied by cooling with a refrigeration cycle, also known as closed-cycle liquefaction [3, 40].

The delivery pressure chosen for the liquefaction process is MP (see Section 3.5.1 for more details on delivery pressure). That is because CO_2 transport at these

conditions has been proven for small quantities, as is the case for Gasendal, and it is already used for food-grade CO_2. If the storage option is chosen, these conditions also correspond to the required delivery by the Northern Lights storage project in Norway [10]. Moreover, CinfraCap, an intermediate storage project in the city of Gothenburg, requires liquefied CO_2 delivery to be slightly subcooled at -28.5°C and 15 barg [43]. Closed-cycle liquefaction is more energy efficient and it is suitable for MP liquefaction [40]. Because of this, a closed-cycle liquefaction process is chosen as the appropriate process design, as can be seen in Figure 4.2.

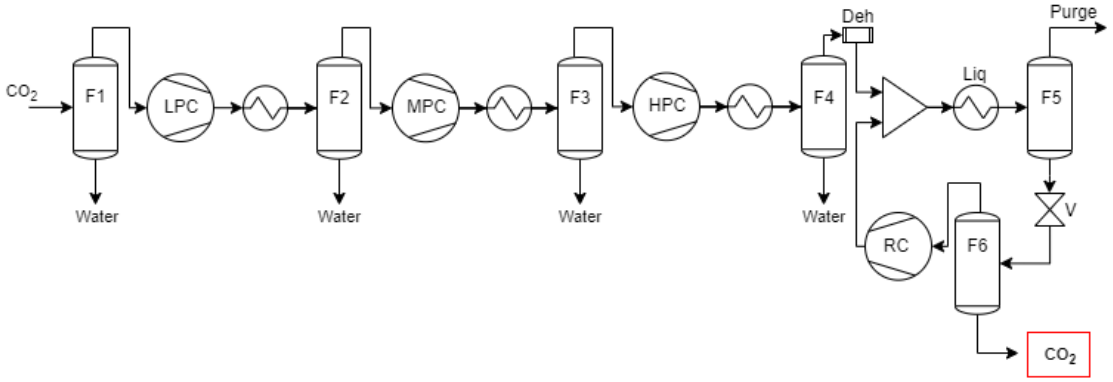

Figure 4.2: General schematics of the CO_2 liquefaction proposed process adapted from [2, 3]

Similar to the utilization plant for e-MeOH, CO_2 first goes into a flash separator (F1) to ensure no liquids go into the compressor. The number of compression stages can be 3 or 4 and generally include intercooling with water removal [2]. The number of stages will depend on which is the optimal design since more stages will increase CAPEX but reduce power consumption. Deng et al. [2] determined an optimal liquefaction pressure of 27.5 bar for a delivery pressure of 15 bar. Therefore, 27.5 bar is set as the final pressure after the compression train, otherwise known as liquefaction pressure. A three-stage compressor train is chosen with an equal pressure ratio for the three compressors. The pressure ratio will be slightly below 3, which is acceptable given that in most compressors the maximum pressure ratio per stage is 4 [46]. This goes in accordance with other authors [2, 3, 40]. The compressors in Figure 4.2 are represented as low-pressure compressor (LPC), medium-pressure compressor (MPC), and high-pressure compressor (HPC). Each stage presents intercooling with water removal through flash separators (F1, F2) including a separator after the HPC (F4) if required.

After F4, CO_2 goes through a dehydrator (Deh) to remove water up to the delivery conditions required by CinfraCap (<30 ppm_v) [43]. Other impurities, such as H_2S should also be removed but this is assumed to be performed efficiently by Gasendal before. Dried CO_2 is mixed with recycled gaseous CO_2 and goes into the liquefier (Liq) which cools and liquefies CO_2 to the delivery temperature of -28.5°C using ammonia (NH_3) as a refrigerant (more details about the refrigeration can be found in Section 4.2.4.1). The Liq block includes a pre-cooler, which operates using cooling water. Block F5 works to remove impurities when partial condensation is preferred

in the liquefier to purge any gas that is not soluble in CO_2 [2]. In this case, such impurities are nonexistent because the CO_2 inlet is assumed pure. The liquid CO_2 from F5 is expanded to the delivery pressure of 15 barg and then goes through another separator (F6) to recirculate gaseous CO_2. Firstly, the recirculated CO_2 goes through a re-compressor (RC) to reach the liquefaction pressure. Liquefied CO_2 is recovered from the bottom of F6. A summary of the input data is shown in Table 4.2.

Table 4.2: Aspen Plus liquefaction simulation input data for the base case

Parameters	ID	Value
Total mass flow rate (kg/h)	m_t	928
Water content at inlet (%wt)	x_{H_2O}	2%
Inlet CO_2 pressure (bar)	P_i	1
Inlet CO_2 temperature (°C)	T_i	23
Liquefaction pressure (bar)	P_{liq}	27.5
Delivery pressure (bar)	P_{del}	16
Delivery temperature (°C)	T_{del}	-29
CO_2 compression train stages	-	3
CO_2 compression pressure ratio	-	3.018
Compressor isentropic efficiency	η_{is}	85%
Intercooling temperature (°C)	T_{cool}	30

4.2.2.1 Carbon dioxide dehydration

The dehydration step portrayed in block Deh from Figure 4.2 is often overlooked since it appears to be a very small step in the complete CCS and CCUS chain. Nonetheless, in order to reach the stringent limit of 30 ppm_v of water content, dehydration seems crucial for most processes. Some pre-combustion capture technologies such as the Rectisol process can deliver a dry CO_2 stream with about 1 ppm_v moisture content [47]. Since amine solutions contain a considerable amount of water, the CO_2 capture using amines very likely always exceeds the limit of 30 ppm_v. Water removal using knockout drums during the compression stages is not enough to remove the required amount of moisture. Dehydration technologies that can achieve concentrations lower than 30 ppm_v of moisture include molecular sieves and TEG (triethylene glycol), but conventional processes based on TEG reach a minimum of 150 ppm_v [47]. Because of this, this work considers molecular sieves for dehydration of CO_2.

Molecular sieve dehydration is an adsorption technology using synthetic zeolite aluminosilicates as the adsorbent agent [47]. Dehydration at higher pressures has proven more efficient and reduces required column sizes using this method [40]. This is why, as also proposed by Deng et al. [2], the dehydration step is set after the high-pressure compressor, which represents the highest pressure level in the process.

To size and be able to estimate the cost of the dehydration unit, the report on *Cost*

critical components in CO_2 capture processes [48] from CEMCAP, a project that studies CO_2 capture from cement production funded by Horizon 2020 [49], is taken as a basis. Detailed cost estimations are presented in the Appendix section A.1.

4.2.3 E-methanol process modelling

The base model developed in this study is based on the flowsheet presented in Figure 4.1. Meunier et al. used the Redlich-Kowong (RK) equation of state and Henry's law for the calculation of thermodynamic properties of the gases [45]. However, the Soave-Redlich-kWong (SRK) equation of state is used in this case, given that it's an appropriate choice for the conditions under which the synthesis of methanol takes place [50]. An isothermal reactor is modeled using an RGIBBS reactor. The simulation of a reactor of this type considers equilibrium conditions given the proposed possible products and doesn't take into account the kinetics of the reaction. Atsonios et al. modeled the process using a Pug-Flow Reactor (PFR) [21]. This is convenient for gas phase reactions since they're easier to control than in other types of reactors, but the reaction kinetics have to be included in the simulation model. Kinetics are not considered in the project, which is why the RGIBBS reactor was chosen. Methanol synthesis runs near the equilibrium [24], justifying the choice for an RGIBBS block. Different authors have considered the use of adiabatic reactors [21,45], but since the reaction is exothermic, temperature control is important.

Heat is considered to be evacuated from the reactor using a cooling jacket with cooling water to maintain a constant reaction temperature. Reaction temperature depends on the equilibrium and kinetics, but existing projects have shown an appropriate temperature of around 230°C [24]. This is also crucial to ensure that the catalyst has reached its activation temperature. To follow the process from Meunier et al. [45], a reaction temperature of 250°C is chosen and kept constant throughout the reaction. The reaction pressure is set to 80 bar, which corresponds to the pressure level used by Meunier et al. and Pérez-Fortes et al. [32, 45].

Compressors are simulated with an isentropic efficiency of 85%. For the base model, cooling duty is assumed to be supplied with cooling water with a 10K temperature difference in the heat exchanger and inlet temperature of 20°C. Heating is supplied by high-pressure live steam, assumed to be provided by the existent boilers at Gasendal. The distillation column is modeled using a DSTW block, and the reflux ratio of the condenser is chosen so as to minimize the number of stages reasonably. Given base case parameters, the effect on different theoretical number of stages and reflux ratios is shown in Figure 4.3 to achieve a molar concentration of 95% MeOH. This is an assumption made given that MeOH can be mixed with water at different proportions to be used as a fuel [51]. Considering that the reflux ratio exhibits no significant decrease beyond 15 stages, the column is designed to have this specific number of stages. The method used for the distillation column simulation is UNIFAC, following the simulation by Meunier et al. [45], while the rest of the model uses the SRK equation of state.

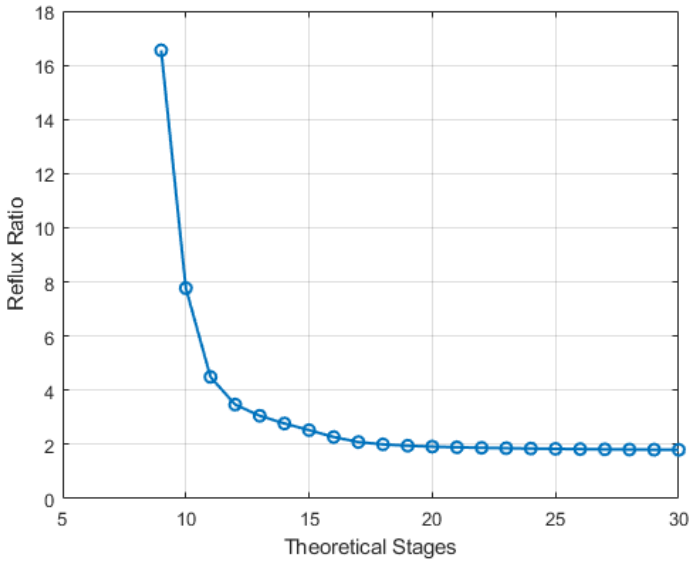

Figure 4.3: Distillation column relation between the number of stages and reflux ratio for the desired purity of 95% methanol on a molar basis

The Aspen Plus flowsheet can be seen in Figure 6.1 in Section 6.1. The four-stage compression of CO_2 is represented by a compression train with intercooling and no liquid removal. Impurities in the product, such as un-reacted H_2 and CO_2 are removed before the distillation column to simplify the distillation design, assuming H_2 can be easily separated from the mixture. The final product could be expected to present small quantities of impurities that are not addressed in this thesis. Other components of the Aspen Plus flowsheet match the design proposed before in Figure 4.1. Water electrolysis through AWE is not simulated but the cost is estimated in the economic analysis.

4.2.4 Liquefaction process modelling

The Peng-Robinsson equation of state is used for the calculation of thermodynamic properties, in accordance with Deng et al. [2]. Similar to the simulation of the utilization plant, compressor isentropic efficiency for the three-stage compression is set to 85%. Since the CO_2 inlet is assumed to be pure with only water and CO_2, there is no purge of impurities in flash F5 because there is complete condensation in the liquefier. Similarly, when expanding the liquefied product to the delivery pressure of 15 barg, there is no gas phase flow so the recirculation can be de-activated. The components are included in the flowsheet to represent the different operation when the flow contains impurities, but are neglected in the cost calculations. There are no losses when removing water during the compression train, so the simulation shows ideal results with 100% of CO_2 liquefied. The dehydration block is simulated with a simple separator, assuming it removes the exact amount of water in order to reach the required limit of 30 ppm_v. The technology proposed to be used for dehydration is a molecular sieve with synthetic zeolite aluminosilicates as it is explained in Section 4.2.2.1. The flowsheet for the process is shown in Figure 6.9, Section 6.2.

4.2.4.1 Refrigeration

The refrigeration cycle is not included in the Aspen Plus simulation but the process is connected to the liquefier heat exchanger shown in Figure 4.2 and Figure 6.9. Ammonia is chosen as the appropriate refrigeration working fluid since its boiling temperature at normal conditions is -33.4°C [52] making it appropriate for the CO_2 liquefaction process. A one-stage refrigeration cycle is proposed because this is able to provide cooling to about -50°C [52]. The process cycle is then represented in Figure 4.4 where the evaporator corresponds to the liquefier.

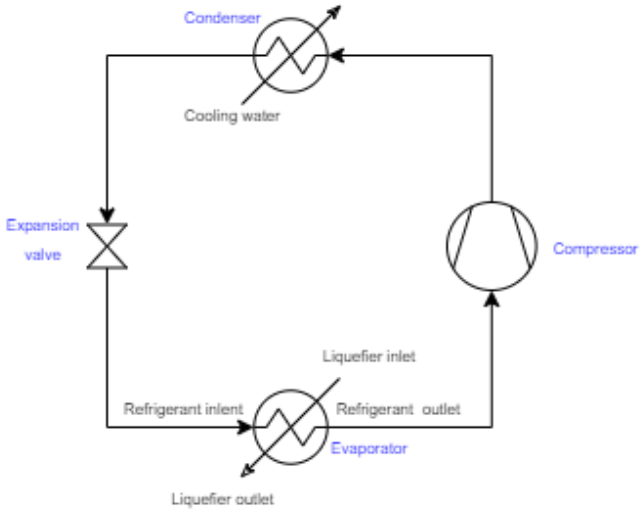

Figure 4.4: One-stage refrigeration basic process (components within the cycle are represented in blue and streams in black)

Sizing of the refrigeration cycle is performed using the CoolPack software, which provides a collection of refrigeration simulation models. The temperature difference of the heat exchangers is set to 5K, as also proposed by Luyben [52]. Phase-change processes, such as evaporation and condensation can easily reach a temperature difference of 5K without the requirement of excessively big heat exchangers. To size the cycle, it is only required to define the temperature levels and the cooling demand. The cooling demand is defined by the Aspen Plus model given the amount of heat evacuated in the liquefier. The temperature of the evaporator in the cycle has to be at least -34°C to be able to cool the CO_2 stream to -29°C and not violate the temperature difference chosen for the design. The condenser temperature is set to 30°C because the cooling is supplied using cooling water. The challenges of having that condenser temperature are further discussed. With a compressor isentropic efficiency of 85%, the P-h diagram can be traced using CoolPack and this is shown in Figure 6.10, Section 6.2.

4.2.5 Heat integration

Heat integration potential is assessed using Aspen Energy Analyzer, which employs pinch analysis techniques. The latter is a method used to optimize the utilization of energy within a process. It allows us to identify the energy targets, assess the potential for heat recovery, and identify energy inefficiencies [53]. In pinch analysis, process streams can be represented in a composite curve, where the temperature levels and heat loads are visible for streams that need to be heated up (cold streams) and cooled down (hot streams). Hot and cold streams can be coupled together to utilize as much energy as possible within the process. The composite and grand composite curves (GCC) are alternative visual representations of the streams that allow reading the minimum external heating and cooling requirements, as well as the heat that can be potentially utilized in the process. Alternatively, the GCC provides information to do a background-foreground analysis where heat recovery to a secondary existing process can be assessed [54]. From the information provided by pinch analysis, a heat exchanger network (HEN) for maximum energy recovery or minimum energy requirement (MER) can be designed. The detailed design of such a network is outside the scope of this study.

The possibility to recover heat within the designed processes, and for the existing Gasendal plant is calculated, especially focused on supplying energy for the CO_2 separation process at Gasendal and quantifying the potential for heat recovery to DH. To perform the analysis, hot and cold streams are extracted from the Aspen Plus and CoolPack simulation. Hot streams are defined as streams that are being cooled and cold streams are those that require heating. The stream start and target temperatures are inputs to Aspen Energy Analyzer, as well as the heat required by those streams, extracted from the net duty calculated for every heat transfer process in the model. Specifically, the duty comes from heat exchangers (including the boiler and condenser at the distillation column) and the heat required to be evacuated from the reactor to keep it at a constant temperature.

From Aspen Energy Analyzer, the energy targets can be extracted to calculate the minimum cost for utilities, in comparison to the base case with no heat integration. The utilities are also included in the analysis. Additionally, the minimum number of heat exchangers for MER is given. Utility assessment is used as well to calculate the amount of heat that can be recovered. Therefore, cooling utilities include Gasendal's existing reboiler (Gasendal RB), assumed to be at a constant temperature of 105°C, DH water, assumed to be heated up from 40°C to 100°C, and cooling water to supply the rest of the cooling demand with an inlet temperature of 20°C. From a former thesis project from Gasendal [15] and confirmation by Göteborg Energi, an average of 700 kW of heat is required in the Gasendal RB. On the other hand, hot utilities will depend on the temperature level required. In the two processes studied, the highest temperature is 250°C, corresponding to the reactor temperature. High-pressure (HP) steam would be required to supply heat at this temperature, and this is assumed to be provided by the existing boilers at Gasendal.

The GCC with utility streams is extracted from the program to provide a visual

representation of the heat recovery potential. Pinch analysis is performed assuming a global minimum temperature difference (ΔT_{min}) of 10K. The optimized ΔT_{min} could be found by cost-optimization, but that goes beyond the scope of this project.

From a former thesis project from Gasendal [15] and confirmation by Göteborg Energi, an average of 700 kW of heat is required in the CO_2 separation.

4.2.6 Equipment sizing

Equipment sizes are taken directly from the process simulations. Flash tanks and the distillation column are sized as vertical pressure vessels. The appropriate size unit for pressure vessels to calculate the cost according to Table 4.3 is the shell mass of the vessel (i.e. the mass of the tank or column). For this it is necessary to consider the design of a vessel under internal pressure in accordance with Towler and Sinnott [55]. The vessel's thickness (t) depends on the internal pressure as described in Equation 4.1.

$$t = \frac{P_i D_i}{2SE - 1.2P_i} \tag{4.1}$$

Where, P_i is the internal pressure, D_i is the internal diameter, S is the maximum allowable stress of the material in pressure units, and E is the welding efficiency, which is considered 100% in this thesis. S is assumed constant for carbon steel with a value of 89 N/mm^2 [8]. Minimum thickness values are reported in the Appendix Table A.1. The shell mass is then approximated as shown in Equation 4.2 [8].

$$Shell\,mass = \pi D_i H t \rho \tag{4.2}$$

Where, H corresponds to the vessel's height or length (m) and ρ is the metal's density, assumed 8000 kg/m^3 for carbon steel. The height and diameter of flash tanks and the distillation column are extracted from the simulation's results.

The heat duty for the heat exchangers is determined based on the simulation results, and the exchanger area is subsequently calculated using Equation 4.3.

$$Q = U * A * LMTD \tag{4.3}$$

Where, Q is the heat exchanger duty in kW, U is the global heat transfer coefficient in kW/m^{2}K, A is the heat exchange area in m^2, and LMTD is the logarithmic mean temperature difference, calculated following Equation 4.4. The value of U used in this study is 1,000 W/m^{2}K for all heat exchangers, following Deng et al. [2].

$$LMTD = \frac{\Delta T_1 - \Delta T_2}{\ln \frac{\Delta T_1}{\Delta T_2}} \tag{4.4}$$

Where, if a counter-current heat exchanger is used, ΔT_1 is the inlet temperature of the hot fluid minus the outlet temperature of the cold fluid, and ΔT_2 is the outlet temperature of the hot fluid minus the inlet temperature of the cold fluid.

4.3 Economic analysis

The method for cost calculations proposed by Towler and Sinnott [8] is taken as a reference to perform the economic analysis. Firstly, the inside battery limits (ISBL) investment is calculated, which includes equipment cost, bulk items (i.e. piping, valves, wires, instruments, structures, paint, lubricants, solvents, and catalysts), civil works, installation labor, construction costs including insurance and other items, such as legal fees, and taxes. Furthermore, offsite costs represent the addition that needs to be added to the ISBL to account for electric substations or power lines, power generation, boilers, steam lines, condensate lines, cooling towers, cooling water lines, water treatment, loading facilities, laboratories, maintenance facilities, emergency services, and security, amongst others. Engineering costs are then added for design and construction, and a contingency charge corresponding to about 10% of ISBL and offsite costs is included [8].

For the pre-feasibility stage of the projects, an order of magnitude cost estimation is performed to estimate capital costs. This is therefore expected to be over- or under-estimated by 30 to 50%. To do this, the cost for major equipment is approximated according to the correlations from Gavin Towler and Sinnott [8]. For both processes proposed, the cost for equipment is estimated using Equation 4.5 [8].

$$C_e = a + bS^n \tag{4.5}$$

Where C_e is the purchased equipment cost, a, b and n are equipment-specific factors found in Table 4.3, and S is the equipment size in the corresponding units.

Table 4.3: Purchased equipment cost correlation factors from [8]

Equipment type	S, units	a	b	n
Centrifugal compressor	Power, kW	8,400	3,100	0.6
U-tube shell and tube exchangers	Area, m^2	10,000	88	1
Double pipe exchangers	Area, m^2	500	1,100	1
Vertical vessels (carbon steel)	Shell mass, kg	-400	230	0.6
Sieve trays for distillation column	Diameter, m	100	120	2

* Note: All costs are in US Gulf Coast Basis from January 2006 (CEPCI 478.6)

The C_e calculated corresponds to 2006 and needs to be updated to account for inflation. This is done using the Chemical Engineering Plant Cost Index (CEPCI) following Equation 4.6.

$$Cost\,year\,A = (Cost\,year\,B)\left(\frac{CEPCI\,year A}{CEPCI\,year\,B}\right) \tag{4.6}$$

Where, in this case, *year A* corresponds to today (i.e. 2023) and *year B* corresponds to the year when the cost is known (i.e. 2006 according to the estimations made using Equation 4.5). Equation 4.6 is also used whenever other costs have to be adjusted to 2023 using the CEPCI factors found in Table 4.4.

Table 4.4: CEPCI values for the years 2006, 2014, 2015, 2021, and 2023

Year	CEPCI
2006	478.6 [a]
2014	576.1 [b]
2015	556.8 [b]
2021	677.1 [b, c]
2023	801.4 [b]

[a] From [8]
[b] From [56]
[c] Taken from April 2021

After C_e is calculated for 2023, all the equipment costs are summed to obtain a total plant purchased equipment cost ($\sum C_e$). Assuming the exchange rate from April 2023 of 1 euro is equal to 1.1 US Dollars, the costs are converted to euros. Then, the factorial method is applied to calculate the ISBL and total fixed capital cost (C_{FC}) taking into account the detailed installation factors presented in Table 4.5.

Table 4.5: Installation factors to estimate the total plant cost from [8]

Item	Description	For fluids
fer	Equipment erection	0.3
fp	Piping	0.8
fi	Instrumentation and control	0.3
fel	Electrical	0.2
fc	Civil	0.3
fs	Structures and building	0.2
fl	Lagging and paint	0.1
ISBL	ISBL=$\sum C_e$*	3.2
OS	Offsites	0.15 [a]
DE	Design and Engineering	0.3
X	Contingency	0.1
C_{FC}	C_{FC}=ISBL(1+OS)(1+DE+X)	
	C_{FC}=ISBL*	1.61

[a] Reduced from 0.3 to 0.15 since the plant is an incorporation of an existing plant that already accounts for some offsite costs. It is assumed that it is appropriate to cut it by half to still consider certain items like additional water cooling, cooling water lines, water treatment, and laboratories.

In summary, what is presented in Table 4.5 means that ISBL corresponds to $\sum C_e$ times 3.2, and C_{FC} is equal to ISBL times 1.61 [8].

Additionally, working capital is added to the fixed cost to account for the cost of starting up the plant for the first time. Given the plants are simple, one-product processes, a low value of 5% of ISBL plus offsites is taken into account to calculate working capital. Variable costs are those that are dependent on e-fuel production or CO_2 liquefaction capacity like electricity, heating, cooling, and the use of other utilities. The electricity price for the base case is set to 66 €/MWh, taken from the Nordpool day-ahead market for price zone SE3, and corresponds to the yearly average for 2021 [57]. From previous experience, cooling water is assumed to cost 0.4 SEK/m^3 and an exchange rate of 11.31 SEK per euro is considered. Finally, as fixed operation costs, operation, and maintenance are assumed to correspond to 5% of the ISBL investment, following the Towler and Sinnott methodology [8] and neglecting other costs.

The C_{FC} is annualized following Equation 4.7. The annualized C_{FC} is also referred to as the annualized investment and is added to the total OPEX to calculate the total annual costs (TAC).

$$a = \frac{i}{1 - (1+i)^{-n}} \tag{4.7}$$

Where, i is the interest rate, and n is the lifetime of the plant. Based on a thesis project performed by Agersborg and Lingehed [15], the economic parameters used by Göteborg Energi for investment projects include an economic lifetime of 15 years for most projects and an interest rate of 7%. The technical lifetime of the equipment might be longer, but the economic lifetime makes references to the accepted payback period [15]. This was confirmed as an appropriate starting point for project economic assessments by Göteborg Energi.

The economic methodology presented is applied identically to both processes studied with the exception of hydrogen production through water electrolysis. Moreover, the reactor for the MeOH synthesis is not calculated following the same methodology as other equipment, since the reactor volume cannot be estimated without considering reaction kinetics. Following Lacerda de Oliveira Campos et al. [58], the purchase costs of the reactor and compressor is assumed to be 75% of the total purchased equipment cost. Given that the cost of the compressors is known, the reactor capital investment can be then estimated. This is done for the base case and not the MER process, where the cost of heat exchangers increases.

4.3.1 Alkaline water electrolysis cost estimation

The AWE process cost was estimated using assumptions found in the literature as reported in Table 4.6. The estimated system cost is derived from predictions that rely on the assumption of AWE investment costs decreasing to a minimum estimated cost of 320 USD/kWe for larger plants. [59]. Similarly, a 4-5 MW plant may cost a minimum of 660 USD/kWe in an estimate for 2025 [59]. Brynolf et al. [60] performed a review on electrofuel production costs and found an intermediate investment value for AWE of 1,100 €/kWe, but this was for 2017. Therefore, it should be lower now. That is why a lower value of 500 €/kWe was assumed. It is considered that this estimate already includes electrical and civil work, design and engineering, and contingency costs. All the other factors from Table 4.5 are applied to the cost calculated to obtain the cost for fixed capital of the electrolysis plant.

Table 4.6: Alkaline water electrolysis system cost and utility/raw material consumption

AWE system cost, utilities and raw material		Utility/raw material costs (€2015/kg) [c]
System cost (€/kWe)	500 [a]	-
Electricity consumption (kWh/kgH_2)	57.9 [b]	-
Deionized water (kg/kgH_2)	10.11 [c]	0.01
KOH (10e-4 kg/kgH_2)	2.75 [c]	2.51
Steam (kg/kgH_2)	0.038 [c]	0.01
Nitrogen (10e-4 kg/kgH_2)	0.7115 [c]	0.28

[a] Assumption from Grahn et al. [19]
[b] Calculated based on an efficiency of 68% on the HHV of H_2 from [6]
[c] From Kuckshinrichs et al. [59]

In terms of electricity consumption, Kuckshinrichs et al. [59] presented a value of 53.9 kWh/kgH_2. With this, the electricity consumption can be calculated based on the produced H_2, which is equal to the required inlet for the methanol synthesis plant. Then, the electricity-to-hydrogen efficiency can be calculated from Equation 4.8.

$$\eta_{electrolysis} = \frac{Energy\ of\ produced\ H_2\ based\ on\ HHV}{Electricity\ consumption} \tag{4.8}$$

Where, $\eta_{electrolysis}$ is the electricity-to-hydrogen efficiency based on higher heating value (HHV). Based on this, the base case would result in 73% efficiency using an HHV of H_2 of 39.4 kWh/kg. This goes in accordance with Reksten et al. [6] for AWE at 1 bar. Nonetheless, the same authors report an efficiency of 68% for AWE at 30 bar, which is the pressure chosen in this study. Therefore, 68% efficiency on HHV is considered in this work to calculate electricity consumption, which results in 57.9 kWh/kgH_2, as reported in Table 4.6.

4.4 Literature cost comparison

4.4.1 E-methanol

The results obtained for the synthesis of e-MeOH are compared to three research papers, each with a different scope. Firstly, Meunier et al. [45] present results on the total costs for an integrated methanol synthesis plant and amine carbon capture unit from cement production. Their production rate is of 1,546 tonMeOH/day, and consider AWE for H_2 production. They show results comparing the effect of including or not the CAPEX of the electrolysis plant, to show the high impact of this. The OPEX of methanol synthesis was 23 €/tonMeOH, while the total production costs, including CO_2 capture and hydrogen production (i.e. considering OPEX only) is 808 €/tonMeOH. The authors reached a break-even electricity price of 34

€/MWh with a MeOH price of 150 €/tonMeOH, and a break-even MeOH price of 843 €/tonMeOH considering an electricity price of 70 €/MWh. The previous results are considering electrolysis CAPEX.

Atsonios et al. [21] present a techno-economic analysis on the synthesis of e-MeOH using industrially captures CO_2 and electrolytic H_2 from AWE. Subtracting the cost of CO_2, the authors reach an e-MeOH cost of 852 €/tonMeOH.

Lastly, Pérez-Fortes et al. [32] study the conversion of CO_2 and H_2 to MeOH for a production of 1,320 tonMeOH/day, excluding capture costs and electrolysis. They assume a price of H_2 of 3,090 €/tonH_2. Their results show a total cost (i.e. including CAPEX, variable, and fixed costs) of 1,117 €/tonMeOH. This results in a breakeven H_2 cost of 1,453 €/tonH_2, or a breakeven MeOH price of 724 €/tonMeOH.

4.4.2 Liquefaction

The current results are compared to three authors. The first one corresponds to Deng et al. [2], given that the process was designed with their research as a basis. The main difference is the price of electricity assumed by the authors which in their case was 80 €/MWh, compared to 66 €/MWh in this thesis. Deng et al. [2] used a cost of cooling water of 0.03 €/m^3. Their results, with the exception of electricity and cooling water costs, were brought from 2015 euros to 2023 euros using the CEPCI, resulting in a liquefaction process cost of 19 €/tonCO_2. Their liquefaction capacity is 1M ton of CO_2 per year.

Secondly, Chen and Morosuk [61] performed an exegetic and economic study on CO_2 liquefaction for 395 ton CO_2 per hour, which corresponds to 3.3M tonCO_2/year. They assumed a project life of 25 years with an interest rate of 7.5%. Their electricity price was assumed as 173 USD/MWh and cooling water 0.029 USD/kWh. Furthermore, they used 2021 as the base year, so by adjusting to 2023, their results show a liquefaction cost of 22.74 €/tonCO_2.

The final research paper used as a comparison was written by Øi et al. [62]. They reported a total capital investment of 23 M€ and OPEX of 4 €/tonCO_2 for a liquefaction capacity of 1M ton of CO_2 per year. The investment was annualized with the same conditions as considered in this thesis to compare the results. Øi et al. [62] used 2014 euros as a reference so the cost was converted to 2023 euros.

In order to compare the final liquefaction cost, the results from this thesis are adjusted to the corresponding utility prices used by the authors. Moreover, for the comparison with Chen and Morosuk [61], the result in this thesis is recalculated to the interest rate and project lifetime used by the authors.

4.5 Sensitivity analysis

This section includes the sensitivity analysis methodology for both processes. The results intend to visualize how certain parameters or conditions may affect the results.

To answer the question of the effect of having a larger plant on project feasibility, the first sensitivity analysis was performed on the effect of inlet CO_2 flowrate on specific process costs. This is done using Aspen Plus to adjust equipment sizes and utility consumption, in order to recalculate costs for both liquefaction and e-MeOH synthesis.

For liquefaction, the liquefaction pressure is chosen as the second sensitivity analysis variable to analyze its effect on total liquefaction costs. This is compared with the results of Deng et al. [2], given that they found an optimal operating condition at a liquefaction pressure of 27.5 bar. For e-MeOH production, the reaction conditions are changed to analyze the effect on CO_2 conversion and costs.

Finally, a sensitivity analysis on electricity prices is performed to study the feasibility of these kinds of projects in the future. For the analysis, the data from Göransson et al. [4] on future electricity prices from Southern Sweden for 2030, 2040, and 2050 is used. The hourly electricity prices are extracted and shown in Figure 4.5. This prediction is obtained from a cost-minimizing electricity system optimization model where CO_2 price increases from 40 €/tonCO_2 in 2030, to 100 €/tonCO_2 in 2040 and 400 €/tonCO_2 in 2050 [63]. The model considers marginal electricity production costs and not the electricity market price, and it assumes that the share of wind power increases from 30% to 60% over the time-frame studied [63].

Figure 4.5 shows how the increase in share for wind power increases the electricity marginal cost variability. It is assumed that the marginal cost of electricity production corresponds to the electricity price and the annual mean electricity price results in 33.10 €/MWh, 49.26 €/MWh, and 50.67 €/MWh for 2030, 2040 and 2050, respectively. The price variability and uncertainty in the future scenarios for the electricity market opens the possibility of future research for Gasendal, and larger CO_2 emitters, to optimize the process. In this thesis, a simple sensitivity analysis on electricity prices is performed assuming constant prices throughout the year.

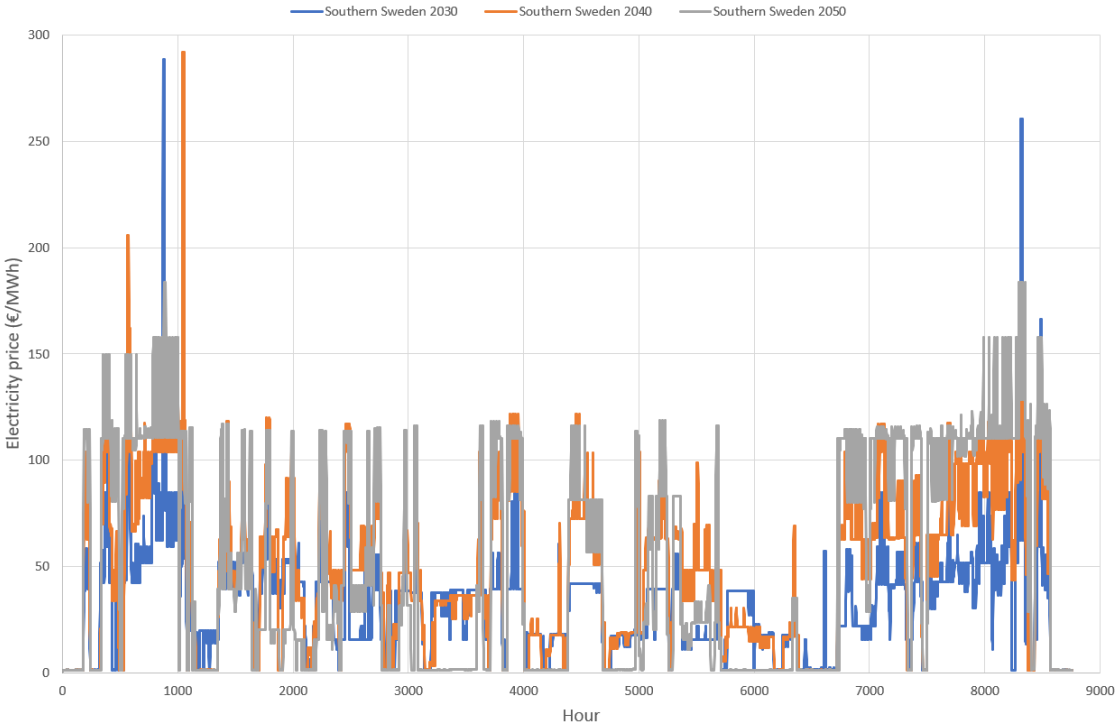

Figure 4.5: Future electricity prices for each hour of a year including 2030, 2040 and 2050 from data by [4]

5

Direct application to the industry and purity requirements

This section will explore the conclusion of a preliminary search for purity requirements and direct utilization pathways based on a report on Biogenic CO_2 from the Biogas Industry by the European Biogas Association (EBA) [5]. Carbonation and packaging in the food and beverage industry, as well as urea production, are examples of well-explored applications of CO_2. Nonetheless, together with urea, EOR is the industrial application with the highest CO_2 demand. Figure 5.1 shows the global demand for CO_2 in 2015 amounting to a total of 250M tonCO_2. This number is expected to increase to 272M tons by 2025.

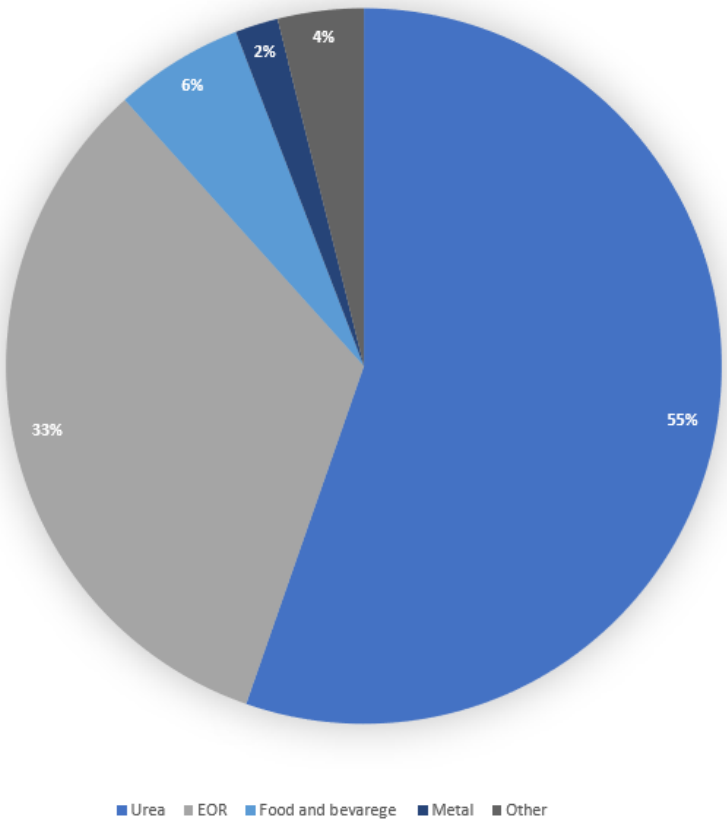

Figure 5.1: Carbon dioxide global demand in 2015 reported in the IEA and extracted from EBA [5]

Common applications include:

- Food and beverage: Packing, carbonation of drinks, deoxygenated water production, or as an acidifier.
- Greenhouse utilization: Increased CO_2 flow in a greenhouse can increase plant growth to 4%. This application, however, is unlikely to be beneficial with high CO_2 prices.
- Fertilizers: Urea has different applications but one of the most common is as a fertilizer. Nowadays, it is still produced mostly from natural gas steam reforming. Biogenic CO_2 is an attractive alternative to produce urea since the CO_2 released would account for net zero emissions.
- Refrigeration: CO_2 is a natural refrigerant with less negative impact when released into the atmosphere compared to other alternatives. If biogenic CO_2 is used, the emission of the refrigerant would be again counted as net zero.

Utilizing CO_2 from biogas presents several advantages. The main contaminant, which is CH_4, is non-toxic. H_2S is removed during upgrading almost in its entirety. Also, the concentration of CO_2 is high with very small quantities of CO since it cannot be present in biogas [5]. Nonetheless, CO_2 captured from a biogas upgrading plant can contain traces of CO and NH_3. There are other advantages presented within the EBA, which include marketing as biogenic CO_2, secured supply, and building synergies in a local bio-economy. In the EBA report, they also present the advantage of price stability, given that biogenic CO_2 doesn't fall within the current carbon market [5]. Nevertheless, as the biogenic CO_2 market emerges, there is an anticipation of a shift, leading to potential volatility in prices. The market's response remains uncertain, adding to the unpredictability.

It is noteworthy to state that future markets are also of interest and include synthetic fuels, polymer manufacturing, semiconductor manufacturing, cultivation of algae, and building materials [5]. Within this thesis, the direct application considers any of the CO_2 utilization pathways, regardless of whether the application includes a conversion process or not, with the exception of e-MeOH as an example of a synthetic fuel. That is because those routes involve only liquefaction and exchange of CO_2 while the integration of an e-MeOH plant is explored separately.

5.1 Purity Requirements

Common impurities in CO_2 from biogas include CH_4, H_2S, CO, alcohols, aldehydes, ketones, aromatic hydrocarbons, NH_3, H_2, N_2 and O_2 [5]. Even if in this thesis impurities are considered negligible, future works and further feasibility studies have to take into consideration the presence of impurities and purity constraints when exchanging or utilizing CO_2.

5.1.1 Food and beverage industry

The E290 standard [64] and the guidelines reported in the European Industrial Gas Association (EIGA) [9] are taken as a reference for food-grade CO_2 coming from

the biogas industry [5]. The E290 standard mainly presents the description of the experimental tests to verify the purity of the CO_2, while the EIGA shows detailed purity standards.

In the E290 standard [64], the content of CO_2 has to be of at least 99% volume on a gaseous basis. To verify CO_2 is within the acidity level, 915 mL of gas have to be bubbled through boiled water and not produce more acid to methylorange when compared to 50 mL of boiled water with the addition of 1 mL of hydrochloric acid (HCl) 0.01 N. To test for reducing substances, hydrogen phosphide (PH_3) and sulfide (H_2S), 915 mL of bubbled CO_2 have to go through 25 mL of ammoniacal silver nitrate ($H_6AgN_3O_3$) that contains 3 mL of NH_3 without clouding the solution. CO_2 cannot contain more than 10 μL/L of CO and no more than 5 mg/kg of oil content [64].

The EIGA [9] presents guidelines that show specific concentration limits for substances in liquid CO_2 used for the food and beverage industry. Table 5.1 shows the CO_2 purity requirement and maximum allowable concentration of different substances expressed in ppm_v, unless otherwise stated. It is noteworthy to state that the purity constraint set by the EIGA is more stringent than that of the E290.

Table 5.1: Carbon dioxide limitations and purity requirement for the food and beverage industry given by the EIGA [9] expressed in ppm volume unless otherwise stated

Component	Concentration
CO_2 Purity	99.9% volume
Moisture	20
Ammonia	2.5
Oxygen	30
Nitrogen oxides	2.5 each
Non-volatile particulates	10 ppm weight
Non-volatile organic residue	5 ppm wight each
Phosphine	0.3
Total volatile HC[a]	50 (20 non-methane HC)
Acetaldehyde	0.2
Aromatic HC[a]	0.02
Carbon monoxide	10
Methanol	10
Hydrogen cyanide	0.5
Total sulfur	0.1
Taste and odor in water and of solid CO_2	No foreign taste and odor
Appearance in water	No color

[a] HC: hydrocarbons

For other CCU and BECCU applications, that is, for direct application in the industry or the integrated e-MeOH synthesis plant, specific requirements may apply,

but the guidelines set in Table 5.1 are generally taken as a baseline [5]. For CCS and BECCS, the Northern Lights project specifications [10] are taken as a reference and that is shown in Table 5.2 in ppm on a molar basis.

Table 5.2: Carbon dioxide composition limitations for storage set by the Northern Lights project [10] expressed in ppm (mol)

Component	Concentration
Moisture	30
Oxygen	10
Sulphur oxides	10
Nitrogen oxides	10
Hydrogen sulphide	9
Carbon monoxide	100
Amine	10
Ammonia	10
Hydrogen	50
Formaldehyde	20
Acetaldehyde	20
Mercury	0.03
Cadmium and thalium	0.03 sum

6

Results and discussion

Results and discussion regarding the technical and economic analysis of the processes are presented in this section. The section starts by exploring all the results concerning the integration of e-MeOH synthesis to Gasendal. Subsequently, the results of the liquefaction process are presented.

6.1 E-methanol

The Aspen Plus simulation flowsheet for the process is shown in Figure 6.1. The main findings and results from the energy requirements are shown in Table 6.1. These results exclude the electrolysis since that was not simulated in Aspen.

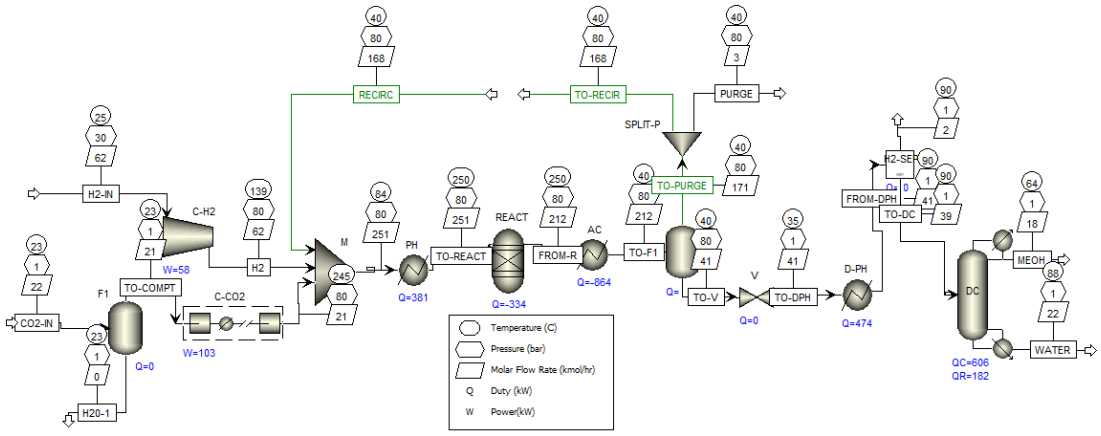

Figure 6.1: Aspen Plus flowsheet for the synthesis of e-methanol

Table 6.1: Energy results for the methanol synthesis (without electrolysis)

Component	Power/Duty (kW)
Cooling	
CO_2-compression train intercooling	55.23
Reaction evacuated heat	334.01
After-cooler	864.34
Distillation condenser	606.89
Heating	
Reaction pre-heater	380.85
Distillation pre-heater	474.36
Disitillation reboiler	183.23
Compression power	
H_2 compression	58.46
CO_2 compression	103.12

The CO_2-compression intercooling duty comes from only two coolers. That is because the temperature after the first compressor is lower than the proposed intercooling temperature of 128°C. No cooling is considered after the high-pressure stage to reduce the heating demand by the reaction pre-heater.

6.1.1 Heat recovery potential

The stream input extracted from the Aspen Plus simulation is shown in Table 6.2. The four-stage CO_2 compression train has only two intercoolers, because of how it was designed, as mentioned before. There is a very high cooling demand, especially in the after-cooler, resulting in a high amount of heat surplus that can be used to cover at least a fraction of the heating demand of the process and reduce the duty in the reboiler from the Gasendal stripper. According to Meunier et al. [45], all the heating demand of the process should be covered while additionally supplying the required heating for the CO_2 stripping process in the CO_2 capture unit.

Table 6.2: Stream input for e-methanol pinch analysis

Stream	Type	Description	T_{start} (°C)	T_{target} (°C)	Q (kW)
H1	Hot	Medium pressure intercooler 1	224.1	128	24.8
H2	Hot	Medium pressure intercooler 2	241.1	128	30.44
H3	Hot	After-cooler after reaction	250	40	864.34
H4	Hot	Distillation condenser	64.21	64.21	606.89
R	Hot	Reactor	250	250	334
C1	Cold	Reaction pre-heater	83.98	250	380.85
C2	Cold	Distillation pre-heater	35.41	90	474.36
C3	Cold	Distillation reboiler	88.41	88.41	183.23

From Aspen Energy Analyzer, the minimum heating demand results in 22.93 kW and minimum cooling demand 844.9 kW. There is a small amount of heat that still needs to be supplied at high temperatures for the reactants to reach the reaction temperature. Since almost all the heating demand is supplied with heat integration, the results are similar to those by Meunier et al. [45]. In terms of cooling, there is a large potential to recover heat to other processes, besides supplying heat within the methanol synthesis. The GCC with the proposed use of cooling utilities of the process is shown in Figure 6.2. Three utility options are present in the graph, high-pressure steam (HP steam), Gasendal RB, and cooling water. There would have been potential to utilize DH as well, but this is excluded since, in this case, the use of the Gasendal RB is favored.

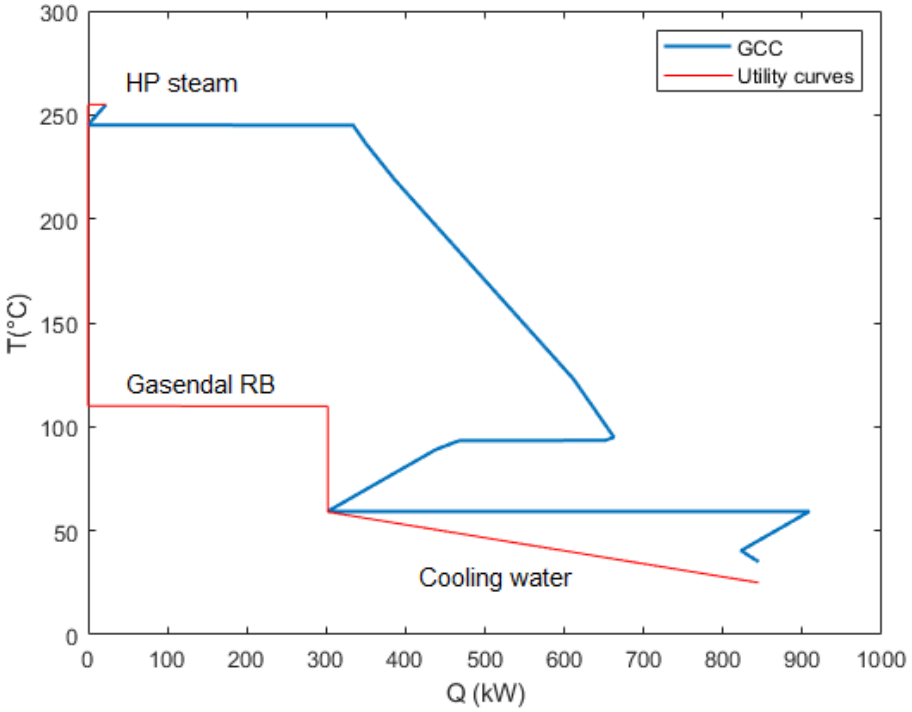

Figure 6.2: Grand composite curve (GCC) for e-methanol synthesis with utility streams. The blue curve represents the GCC of the process and the red curve shows the utility options to supply heating and cooling

HP steam is set to a temperature of 260°C, in order to supply heat up to 250°C. Gasendal RB is at a temperature of 105°C and provides cooling up to the pocket, as shown in the GCC. The rest of the cooling demand is supplied with cooling water coming in at 20°C. Cooling water can be heated up to a temperature of 54°C, where it crosses a utility pinch point. The heat targets for each of the utilities are shown in Table 6.3.

Table 6.3: Utility supply options for e-methanol synthesis

Utility supply options	Q (kW)
Gasendal RB	302.20
Cooling water	542.80
HP steam	22.93

The MER HEN is not traced in detail, but the MER network results in a minimum number of heat exchangers of 11. The minimum heat transfer area is 50 m^2. The differences in capital costs are shown in Table 6.4. In terms of heat recovery to the existing process, 302.2 kW can be recovered to be used in the reboiler of Gasendal. If the reboiler requires 700 kW, 43% can be supplied by the e-MeOH process reducing the required reboiler duty to 397.8 kW.

6.1.2 Economic analysis

In terms of CAPEX, the cost comparison for adding heat exchange units to reach MER is shown in Table 6.4, where the base case is the process simulated with no heat integration, and the heat integrated case results from performing pinch analysis shown in Section 6.1.1. Note that these results exclude water electrolysis, and the investment cost shown corresponds to the entire plant.

Table 6.4: CAPEX for e-methanol synthesis with and without heat integration

Case	Number of HEX	Transfer area (m2)	Purchased cost	C_{FC}
Base	5	28.77	631 360 €	3.25 M€
Heat integrated	11	50	725 538 €	3.74 M€

Regarding variable OPEX, the cost savings by integrating the process are shown in Table 6.5. The savings in total OPEX result in 1.9 M€. This was performed considering a high cost of natural gas of 0.2 €/kWh and can be adjusted to lower prices. Nonetheless, the heating savings are of a considerable amount of 98%, as shown in Table 6.5. This goes in accordance to Meunier et al. [45], who concluded that 100% of the required heat in the process could be supplied by heat integration, because of the large amount of heat surplus available. Table 6.5 does not show electricity costs, as this remains the same with and without heat integration.

Table 6.5: Variable OPEX for e-methanol synthesis with and without heat integration

Case	Heating (kW)	Cooling (kW)	Variable OPEX	Fixed OPEX
No heat integration	1038.44	1860.48	1.94 M€	101 018 €
Heat integrated process	22.93	542.80[a]	68 529 €	116 086 €

[a] Assuming that the additional 302.20 kW of cooling are supplied by Gasendal RB

Considering the increase in CAPEX shown in Table 6.4, the savings in TAC still sum up to 1.8 M€, justifying the need to include heat integration. Furthermore, the Gasendal RB heat duty reduction to 397.8 kW (saving 302.20 kW) amount to around 0.5 M€ of additional savings per year for Gasendal, if the same natural gas price is considered. Further results are shown only for the energy-integrated process, since the OPEX savings far outweigh the increase in capital cost. The CAPEX breakdown from the result shown in Table 6.4 is shown in Figure 6.3.

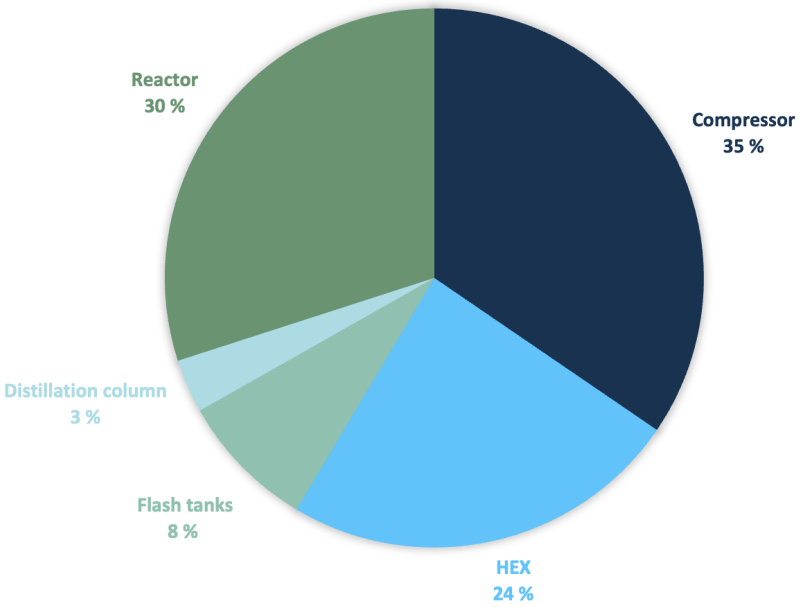

Figure 6.3: Capital cost distribution by equipment type for the energy-integrated methanol synthesis, not including electrolysis costs. HEX represents heat exchangers in the synthesis process including the condenser and boiler from the distillation column

The compressors and reactor constitute 66% of the total capital costs for the e-methanol synthesis, excluding electrolysis. Heat exchangers are 23% of costs, taking into account the cooling jacket in the reactor. Lastly, the distillation column, including plates and the flash tanks is 11% of the total installed investment.

Water electrolysis installed cost, so-called C_{FC}, or cost for fixed capital, is 11.28 M€, considerably higher than that of the e-methanol section. Electrolysis raw material and utility consumption, with their respective costs, are shown in Table 6.6. The vast majority of utility and raw material expenditure goes to electricity, accounting for 96% of the total variable OPEX. Water consumption takes 4%, and the other raw material expenses are negligible.

The total cost summary for e-MeOH synthesis with hydrogen production is shown in Table 6.7. Hydrogen production is, by far, the most expensive part of the process with a cost of 1,259 €/tonMeOH. The specific cost of hydrogen for the process is 5.63 €/kgH_2. Figure 6.4 shows the cost distribution per ton of e-MeOH produced

divided into electrolysis, CAPEX, and OPEX (CAPEX and OPEX only represent costs for the MeOH synthesis without electrolysis). 91% of total e-methanol costs are because of the production of hydrogen and, therefore, water electrolysis remains the bottleneck for the synthesis of e-methanol.

Table 6.6: Electrolysis variable OPEX breakdown

Utilities and raw materials	Consumption per year	Cost per year
Electricity (MWh)	61,206	4 M€
Deionized water (ton/a)	10,679	153 713 €
KOH (ton/a)	2.90	23 061 €
Steam (ton/a)	40.14	578 €
Nitrogen (ton/a)	0.75	301 €
	Variable OPEX	4.22 M€

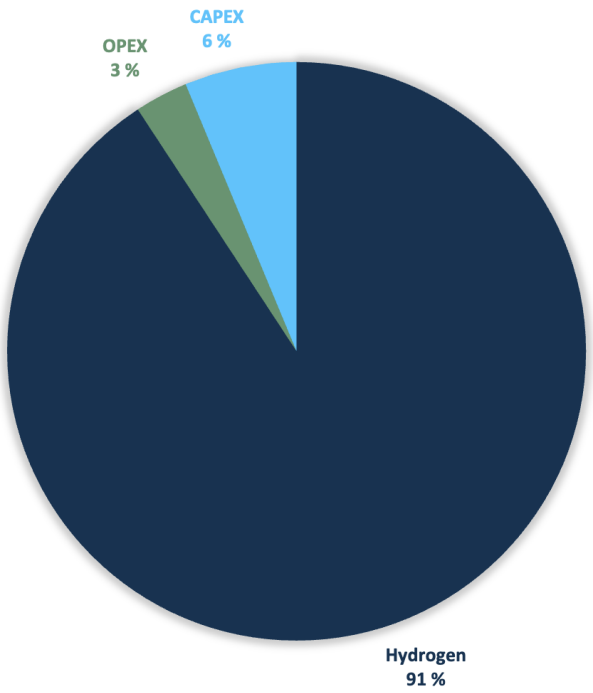

Figure 6.4: E-methanol total production cost distribution, including hydrogen production through AWE and the OPEX and CAPEX of the CO_2 hydrogenation to methanol process

As a business case, with the costs calculated, the minimum selling price for e-MeOH should be 1.39 €/kgMeOH to reach an annualized net profit of zero. If instead the market price of fossil methanol is considered as 0.495 €/kgMeOH [58], the break-even cost for hydrogen production should be 1.64 €/kgH_2, which is 3.99 €/kgH_2 lower than the estimated cost for this project.

High incentives are required to make e-fuel synthesis a feasible option for Gasendal. A minimum economic incentive of 3.99 €/kgH_2 would be required, taking into account the amount of hydrogen required given the CO_2 flow from Gasendal. Otherwise, an incentive of 0.895 €/kgMeOH should be given according to the quantity of net zero e-MeOH sold. Alternatively, the price of e-MeOH should be at least double to reach a break-even point. Figure 6.8 shows a more detailed image of the impact of H_2 cost or price on total MeOH production costs.

Table 6.7: E-methanol and electrolysis total plant cost

Total cost summary	E-methanol	Electrolysis
Annualized C_{FC}	410 410 €	1.2 M€
Working capital	133 499 €	563 934 €
Variable OPEX	79 193 €	4.2 M€
Fixed OPEX	116 086 €	490 378 €
Total Annualized Cost (TAC)	605 689 €	5.9 M€
Specific process cost (€/tonMeOH)	128.27 €	1 259.19 €

These conclusions are limited since optimized H_2 production and storage are not taken into account. Rather, the analysis assumes a constant electricity price of 66 €/MWh and continuous operation. Future studies should include an optimization model to consider hydrogen production and synthesis when the electricity price is low. Excess hydrogen production could potentially, although it's probably unlikely, ensure constant hydrogen supply to the e-MeOH synthesis if optimized storage is designed. Alternatively, e-MeOH synthesis would not be a continuous process and e-MeOH would be produced when electrolysis is operating at low electricity prices, or when there is hydrogen still in storage. A system-oriented optimization model could assist this process-focused thesis to determine optimal e-fuel synthesis conditions. Furthermore, the high costs should also be associated with the small-scale plant. Therefore, the upscaling of the process is assessed within the sensitivity analysis.

E-MeOH total production costs resulted in 1,387 €/tonMeOH, which is 63% and 24% higher than that reported by Atsonios et al. [21] and Pérez-Fortes et al. [32], respectively. Nonetheless, Pérez-Fortes et al. [32] use a fixed H_2 cost of 3,090 €/tonH_2. Assuming H_2 is bought at that price for this thesis results in a lower cost of 820 €/tonMeOH. That result is also reflected when the H_2 break-even price or cost is compared. Pérez-Fortes et al. [32] obtained a break-even cost of 1,453 €/tonH_2, while in this thesis H_2 could have a higher cost of 1,639 €/tonH_2 to break-even.

Using an electricity price of 66 €/MWh, the MeOH break-even price in this project is 1,387 €/tonMeOH, equivalent to the total annual production costs. That is 64% and 92% higher than that obtained by Meunier et al. [45] and Pérez-Fortes et al. [32], respectively. Pérez-Fortes et al. [32] report, however, a lower methanol break-even price than the cost reported.

The higher cost obtained in this project could initially be attributed to economies of scale, but that has to be confirmed with a sensitivity analysis shown in Section 6.1.3. Here it can be seen that in this case, economies of scale might not be the reason for the differences. Since the highest cost is that of electrolysis, the difference has to be attributed to the assumptions made to calculate the cost of the process.

6.1.3 Sensitivity analysis

The first sensitivity analysis results presented are regarding the effect of having a larger plant, that is, a higher level of emissions at the CO_2 source plant. The results are shown in Figure 6.5, and are divided into MeOH synthesis costs and electrolysis costs for hydrogen production. Note that the cost of electrolysis, since it is considerably higher, is shown in the secondary Y-axis.

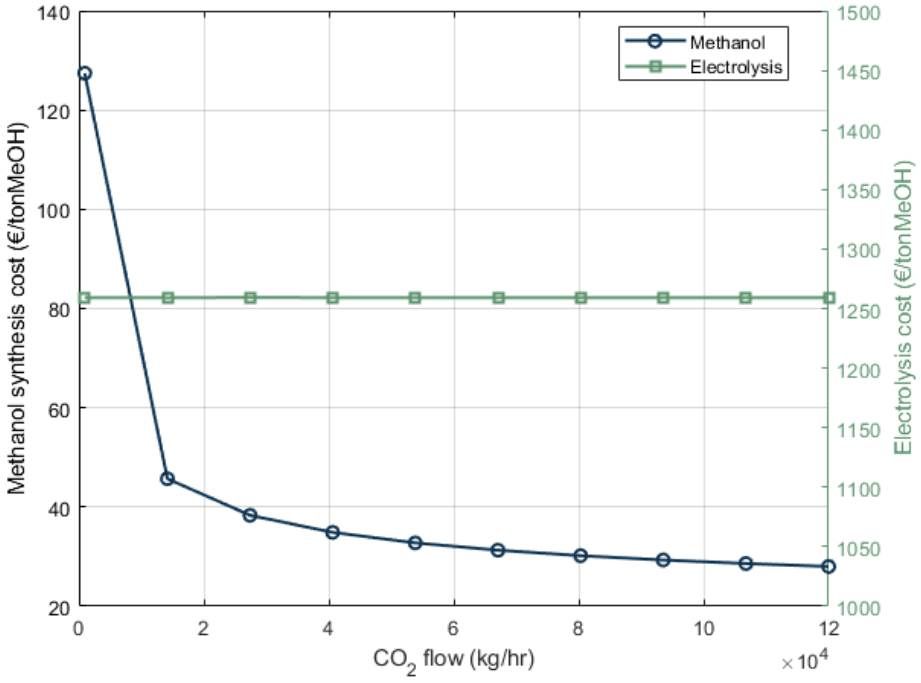

Figure 6.5: E-methanol production cost when varying the CO_2 inlet flow. The Y-axis on the left represents the costs for methanol synthesis and Y-axis on the right represents the costs for water electrolysis

MeOH synthesis costs can be considerably reduced from that calculated for Gasendal to around 30 €/tonMeOH for a plant with 1M ton of CO_2 emissions per year. The cost reduction would be of around 100 €/tonMeOH, which seems considerable. Nonetheless, electrolysis costs seem to remain constant at higher CO_2 flows. That is because the capital costs and electricity consumption per ton of H_2 produced are assumed to remain constant. Unfortunately, at this point of the study, it cannot be argued that AWE capital cost will decrease with larger H_2 production. The data reported by Reksten et al. [6] on capital AWE costs is shown in Figure 6.6. For a capacity of 5 MW and higher, the CAPEX costs appear to level off at values

exceeding 500 €/kWe. The capacity of the electrolysis plant required for Gasendal is of 7.2 MW to produce 125 kg/h of H_2.

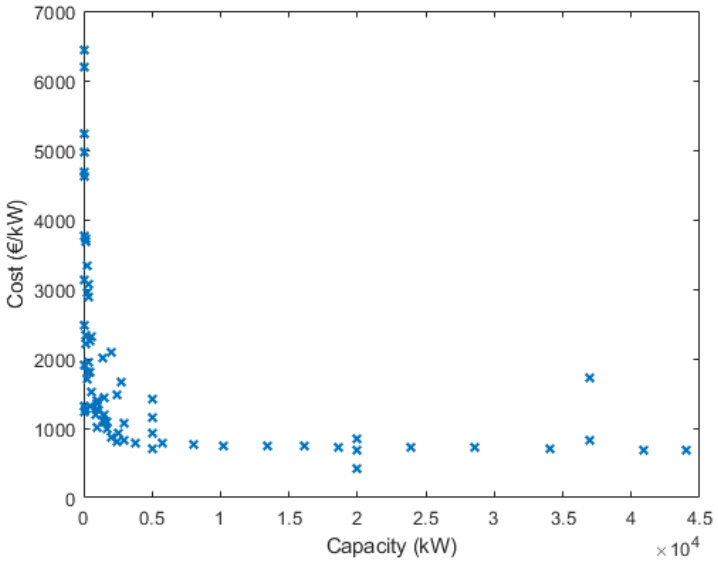

Figure 6.6: Cost review data representation on electrolysis CAPEX from the data by [6]

6.1.3.1 Future electricity market price projection sensitivity

The effect that electricity price variations have on e-methanol cost is shown in Figure 6.7. The cost is considerably sensitive to electricity prices, mainly because of the electricity demand in hydrogen production. Nonetheless, an electricity price lower than 20 €/MWh would be needed to reach a break-even cost level.

Electricity prices affect electrolysis the most. Then, another way of representing this analysis is by performing a sensitivity analysis on hydrogen price, or cost, which is shown in Figure 6.8. Buying fossil H_2 from the market would lead to a very small profit margin, as can be seen from Figure 6.8. The vertical red line shows almost break-even production costs as it crosses the e-MeOH production cost curve almost at the same point as it crosses the MeOH market price. There needs to be further clarity on the terms, however, since this would no longer be e-MeOH production, but just MeOH synthesis.

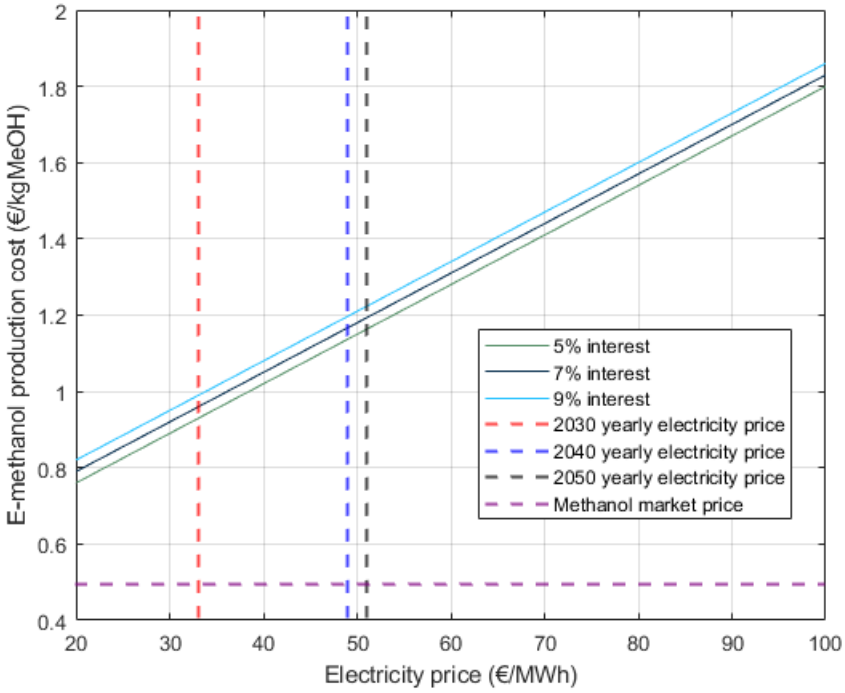

Figure 6.7: Effect of different electricity prices on e-methanol cost for different interest rate cases

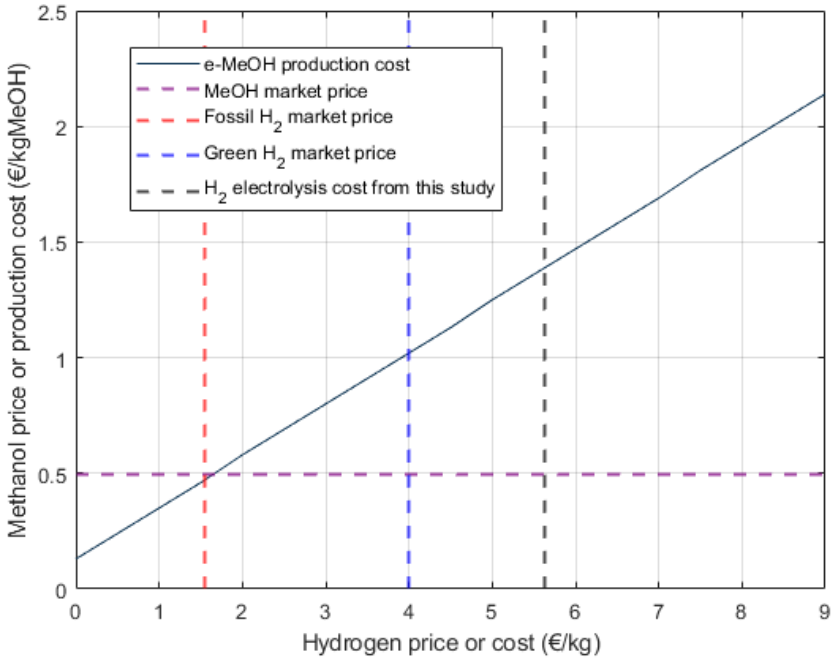

Figure 6.8: E-methanol production cost when varying H_2 price. Dashed lines indicate the methanol market price, fossil hydrogen market price, estimated green methanol market price, and this study's result on hydrogen production cost

To produce e-MeOH, green hydrogen from electrolysis has to be bought, or produced. If green H_2 is bought at market price (vertical blue line from Figure 6.8), the cost of eMeOH would need to be 1 €/kgMeOH to break even. For the Gasendal case, the production of H_2 from AWE costs more than buying it. Therefore, it is suggested to buy green hydrogen instead of producing it. Nonetheless, it is noteworthy to mention that it was previously concluded that electrolysis costs do not decrease with plant capacity. Hence, electrolysis costs in this study might be overestimated. That is because it is assumed that the electrolyzer operates continuously, instead of optimizing hydrogen production at lower electricity prices.

Future work should consider analyzing the effect of optimizing hydrogen production, which should shorten the distance between the calculated costs of hydrogen synthesis through AWE and the current green hydrogen market price. The results are therefore not conclusive, but provide an initial foundation to argue that such a project can break even at an e-MeOH selling price of around 1 €/kgMeOH, if H_2 is produced or bought at 4 €/kgH_2. Considering that a price of 1 €/kgMeOH for e-MeOH is not unreasonable, a project of this nature has the potential to serve as a great pilot project.

6.2 Liquefaction

Based on the base model shown in Figure 6.9, with the input presented in Table 4.2 including a liquefaction pressure of 27.5 bar and a delivery pressure of 16 bar, the energy requirements for the process are presented in Table 6.8.

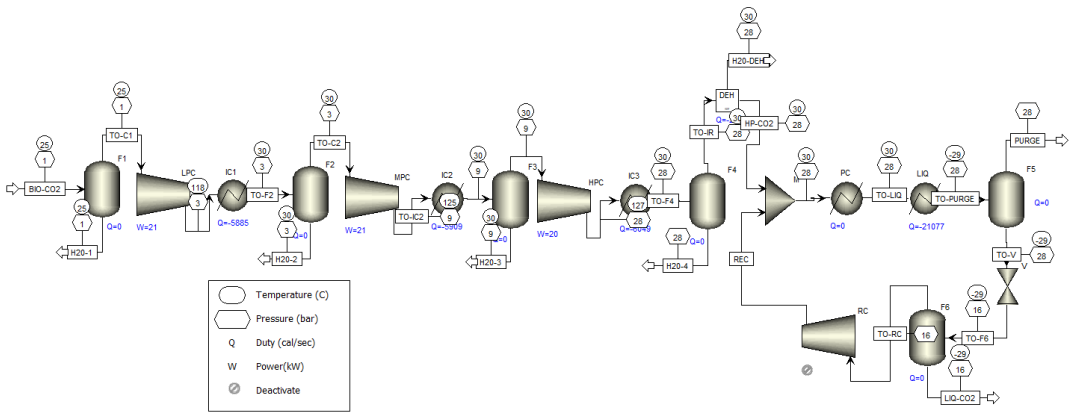

Figure 6.9: Aspen Plus flowsheet for the liquefaction of CO_2

Table 6.8: Energy results for the liquefaction process

Component	Power/Duty (kW)
CO2 compression train	62.71
Refrigeration compression	36.51
Recycle compression	0
Cooling demand	198.60
Liquefier cooling demand	88.24
Heating demand	0

Given the liquefier duty of 88.24 kW and the temperature levels for the refrigeration cycle explained in Section 4.2.4.1, the P-h diagram extracted from CoolPack is shown in Figure 6.10. This represents a one-stage compression cycle. Important parameters can be extracted from this plot, which will be relevant when performing pinch analysis.

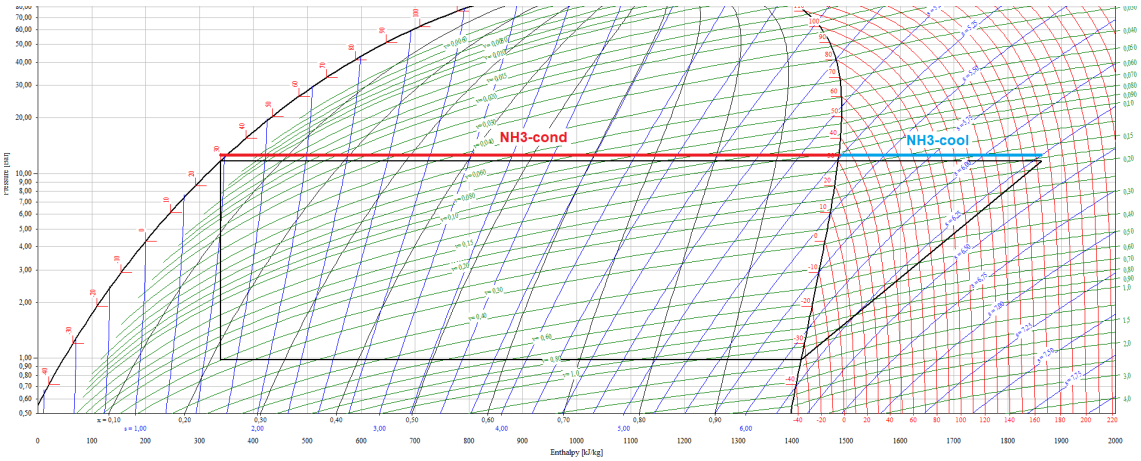

Figure 6.10: Ammonia refrigeration P-h diagram for the base case

The liquefaction process has no heating demand and only cooling is required. Intercooling and cooling after the compression train is done using cooling water. With a cooling demand of 200 kW, including cooling from the condenser of the ammonia refrigeration cycle, there is a heat surplus that can potentially be utilized. Heat recovery potential is assessed in Section 6.2.1.

6.2.1 Heat recovery potential

Within the process, there is cooling demand in the intercooling within the compression train and in the condenser of the ammonia cycle. The input streams are presented on Table 6.9, where IC1, IC2, and IC3 represent the coolers within the CO_2 compression train. For the NH_3 cycle, in the condenser the stream is separated into two streams: NH_3-cool for the cooling of ammonia to the saturation temperature (sensible heat), and NH_3-cond for the condensation of ammonia at 30°C (latent heat). The temperature values and cooling demand (Q) are extracted

from the Aspen Plus simulation. From the results provided by CoolPack, the total condenser heat load can be extracted. This can be further divided into two streams by extracting the enthalpy values from the NH_3 P-h diagram shown in Figure 6.10 and multiplying it times the NH_3 mass flow rate.

Table 6.9: Stream input for liquefaction pinch analysis

Stream	Description	T_{start} (°C)	T_{target} (°C)	Q (kW)
IC1	Low pressure intercooler	114.6	30	22.83
IC2	Medeum pressure intercooler	123.5	30	24.45
IC3	High pressure cooler	129.1	30	26.57
NH_3-cool	Ammonia cooling to saturation	173.7	30	31.06
NH_3-cond	Ammonia condensing	30	30	93.69

The GCC is shown in Figure 6.11, where, as already mentioned repeatedly, there is only a cooling demand of just below 200 kW, so the system is unpinched. However, there is a potential for heat recovery within the heat surplus of the system. In the GCC, the blue lines show the cooling utilities available, including using heat directly Gasendal RB, using the heat for DH, or using cooling water coming in at 20°C.

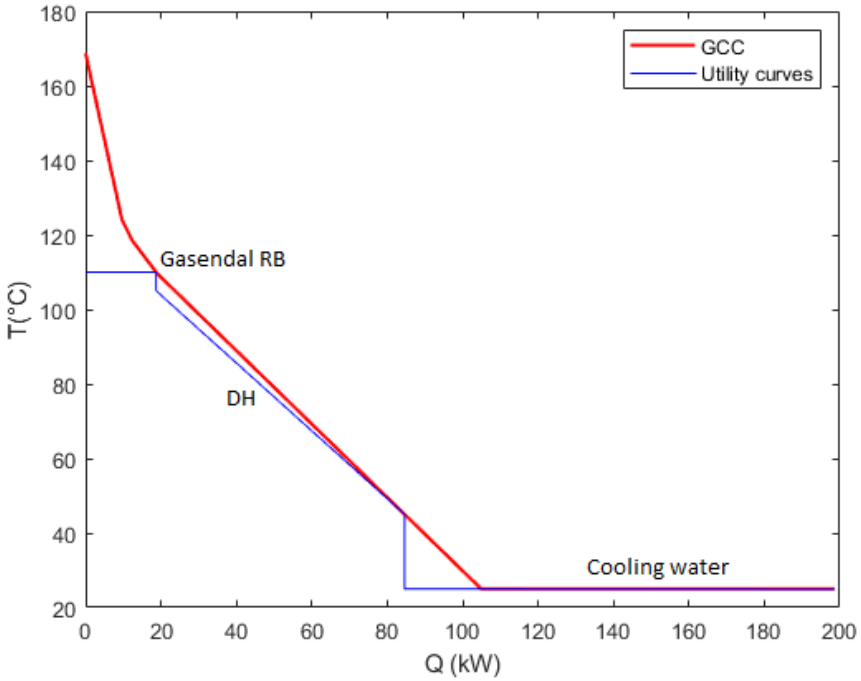

Figure 6.11: Grand composite curve (GCC) for CO_2 liquefaction with utility streams. The red curve represents the GCC for compression and liquefaction of CO_2 and the blue curve shows the utility options including Gasendal RB, DH and cooling water

The heat loads that can be evacuated from the process are represented graphically in the GCC of the process and shown in Table 6.10

Table 6.10: Cooling supply options for CO_2 liquefaction

Cooling supply options	Q (kW)
Gasendal RB	18.70
DH	65.91
Cooling water	113.99

From the 700 kW required by the Gasendal RB, only 2.7% can be recovered from liquefaction. A detailed cost analysis for this is not performed but it is assumed that the heat recovery potential is so small that it wouldn't be feasible to consider recovering the heat surplus to reduce the current heating demand from Gasendal. From the GCC, it is then possible to conclude that the cooling supplied by Gasendal RB can be instead supplied by additional DH water, resulting in a total DH heat recovery potential of 84.61 kW. From direct information provided by Göteborg Energi, there is no close connection to the DH network, which would make it unreasonable to think of an investment in a DH connection to recover a considerably small quantity of heat. Nonetheless, the potential for heat recovery is still mentioned.

The additional 114 kW of cooling has to be supplied with cooling water. As can be seen in the GCC from Figure 6.11, cooling water is mostly required for a phase change process, corresponding to the condensation of NH_3 at a temperature of 30°C in the refrigeration cycle. Taking into account a supply of cooling water at 20°C, coming from air cooling, which is the water cooling method at Gasendal, the only way to avoid violating the ΔT_{min} of 10K is to have an infinite mass flow rate of water. Hence, the cooling water supply line shown in the GCC is a horizontal line with inlet and outlet temperature equal to 20°C. In practice, this is not possible. Given that a supply cooling water temperature lower than 20°C is unlikely, even in winter, a realistic approach would be raising the temperature of the condenser in the NH_3 cycle. A ΔT_{min} of 5K is possible in a condenser, so increasing the condensation temperature to 40°C would be a viable approach, considering a cooling water temperature increase from 20°C to 25°C. This would, in turn, decrease the refrigeration efficiency.

6.2.2 Economic analysis

The process is divided into three parts to summarize costs. The first component is the CO_2 compression train, including the first flash separator, intercooling heat exchangers, intercooling flash tanks, high-pressure cooler, and high-pressure flash tank. The second component is the NH_3 refrigeration cycle, including the liquefier. Lastly, the dehydrator costs are included. Note that F5, F6, and RC are not included, since they are de-activated when having a pure inlet CO_2 stream. When conducting future cost analysis, it is important to recognize that the RC has the potential to significantly raise expenses. The equipment purchased cost and the total cost for fixed capital are shown in Table 6.11. The largest expenses are corresponding to the CO_2 compression train, followed by the NH_3 refrigeration cycle.

Table 6.11: Capital costs for basic liquefaction process components

Component	Purchase cost	C_{FC}
CO_2 compression train	193 312 €	995 943 €
NH_3 cycle	78 329 €	403 551 €
Dehydrator	2 737 €	14 100 €
Total cost	274 378 €	1.4 M€

To further analyze the impact of each equipment type on the total CAPEX, the equipment of the process is divided into compressors, flash tanks, heat exchangers (HEX), and the CO_2 dehydrator. The contribution of each equipment type to the total capital cost, assuming equal installation factors for every component is shown in Figure 6.12.

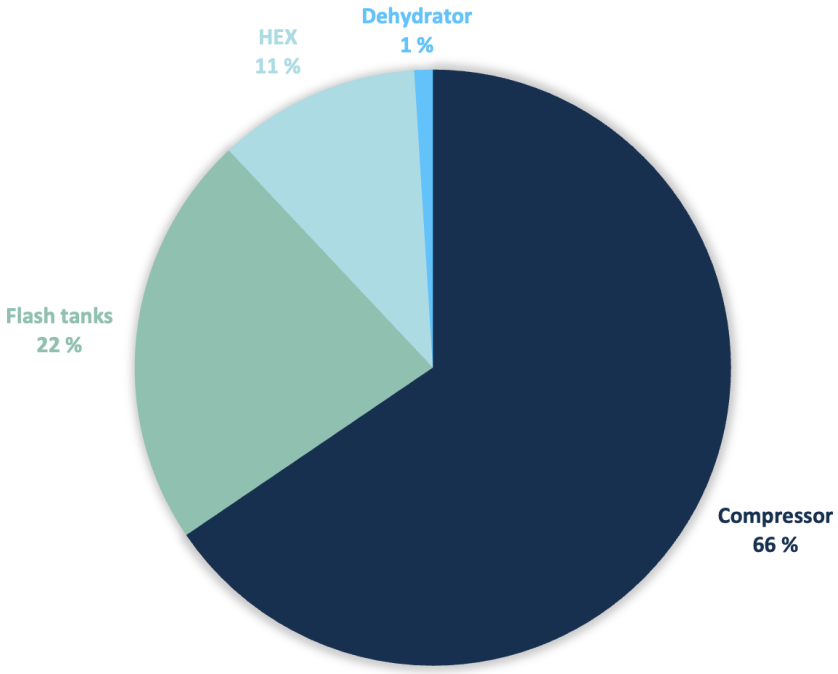

Figure 6.12: CAPEX distribution by equipment type for the compression and liquefaction of CO_2. HEX represents all the heat exchangers in the process

The capital cost for a dehydration unit represents only 1% of the total CAPEX. It can then be concluded that for initial feasibility studies, this cost can be considered negligible. The major contribution to capital costs comes from the compressors. This is not unexpected as the entire liquefaction process involves multiple compression stages. Furthermore, compressors involve a lot of moving parts, making them expensive. Flash tanks and heat exchangers represent 22.50% and 11% of the total CAPEX, respectively. To avoid re-sizing heat exchangers and flash tanks with the sensitivity analysis, these percentages of the total CAPEX are fixed for further results, and the dehydrator is considered negligible.

The utility consumption and variable OPEX are presented in Table 6.12 and the summarized annual costs per ton of liquefied CO_2 are shown in Table 6.13.

Table 6.12: Operational costs

Utility	Consumption per year		Cost per year
Electricity	836	MWh	55 171 €
Cooling water	288,211	m^3	10 193 €
Variable OPEX	-		65 364 €

Table 6.13: Annual liquefaction cost and total specific liquefaction cost per ton of CO_2

Liquefaction cost summary	
Annualized C_{FC}	155 205 €
Variable OPEX	65 364 €
Fixed OPEX	43 900 €
TAC	264 470 €
Liquefaction cost (€/tonCO_2)	34.43 €

The total specific liquefaction cost for Gasendal is 34.43 €/tonCO_2, assuming the only impurity is water. CO_2 is dried so that the liquefied CO_2 has a concentration of 30 ppm_v of water. Because of the CO_2 purity assumptions, the re-compressor and flash tanks F5 and F6 are not considered in the simulations. That means that the cost is underestimated. Furthermore, costs for storage on-site are not included and CO_2 transport to the end-user or storage facility goes beyond the scope of this study. A volume of CO_2 as the one studied would only require truck and train transport. The capacity of transport can be considered to be 38 tonCO_2 per truck [65]. The liquefaction of 928 kg/h, assuming continuous operation, corresponds to 22.3 tonCO_2/day. Thus, only one truck per day would be required. Regarding on-site storage, it may be worth considering a two-day storage period in future projects to accommodate potential disruptions during weekends or any issues that may arise with the truck or train.

A comparison with other studies with similar conditions is presented in Table 6.14. The first column is the cost reported by the authors, updated to 2023 Euros. The second column represents the costs from this study updated to the conditions of the authors to which the comparison is made.

Table 6.14: Liquefaction cost comparison to that reported in the literature

Reference	Updated Cost (€/tonCO_2)	Gasendal updated (€/tonCO_2)
Deng et al. [2]	18.99 €	36.70 €
Chen et al. [61]	22.74 €	41.75 €
Øi et al. [62]	9.65 €	33.28 €

The cost of liquefaction per ton of CO_2 of this study for Gasendal is at least 80% higher than that reported by the other authors. It is believed that one of the main reasons for this is because of economies of scale, that is, Gasendal has a very low level of CO_2 emissions. This is analyzed in the sensitivity analyses presented in Section 6.2.3. A further comparison is performed with Deng et al. [2], given that the process studied is inspired by their research. This is shown in Figure 6.13. It is clearly displayed that the biggest specific liquefaction cost difference relies on the CAPEX costs. Capital expenses per ton of CO_2 would be expected to decrease for larger plants because of economies of scale.

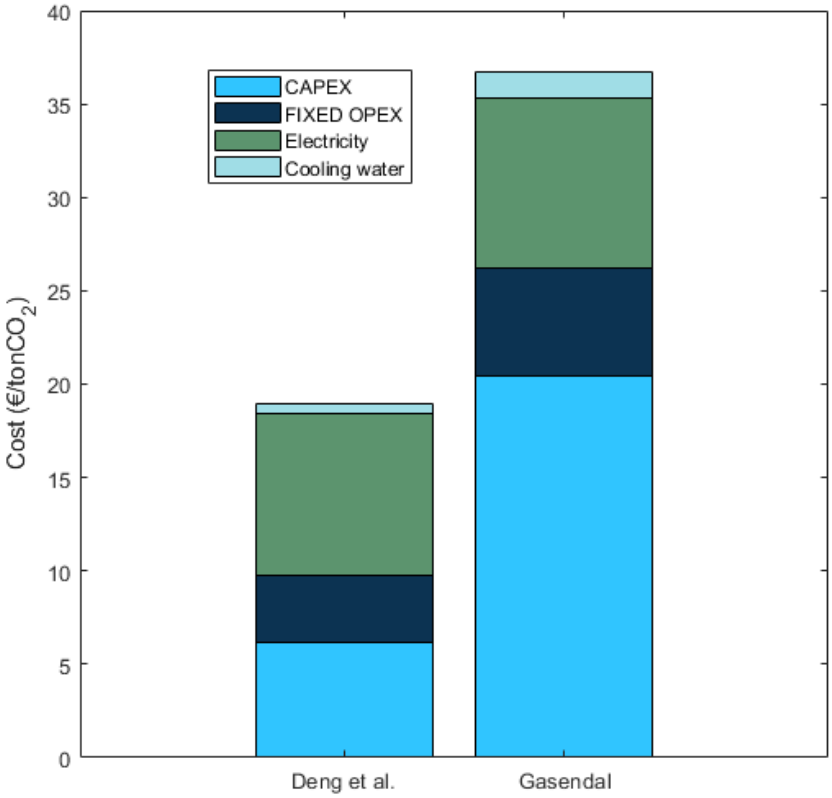

Figure 6.13: Total specific liquefaction cost for Gasendal compared with the results from Deng et al. [2] divided in CAPEX, Fixed OPEX, electricity costs, and cooling water costs

.

6.2.3 Sensitivity analysis

The result of increasing the plant size in terms of specific liquefaction costs is presented in Figure 6.14. With an emission level of around 950,000 tons of CO_2 per year, the specific cost for CO_2 liquefaction goes down to 10.50 €/tonCO_2. This value is now comparable to that reported by Øi et al. [62] for a similar emission level. Øi et al. [62] perform the study for 1 million tons of CO_2 per year. Scaling up the process would, as expected, reduce specific costs and increase the feasibility of the project.

For a project like this, subsidies, and incentives have to be valued according to the need to supply biogenic CO_2 as feedstock to other processes to displace the use of fossil resources. It is difficult to argue that small facilities like Gasendal will receive negative emission incentives, as these incentives are likely to be targeted towards larger emitters with lower specific costs. It is then important to prioritize the development of BECCS for biomass and waste combined heat and power plants, as well as implementing CCS in industries such as pulp and paper, metal, and construction materials. Considering this, industries emitting smaller amounts of biogenic emissions could potentially advocate for greater incentives per ton of CO_2 based on the extent to which they displace fossil CO_2 in other industries through the pathway categorized in this study as the direct application of CO_2 to the industry, rather than relying on storage.

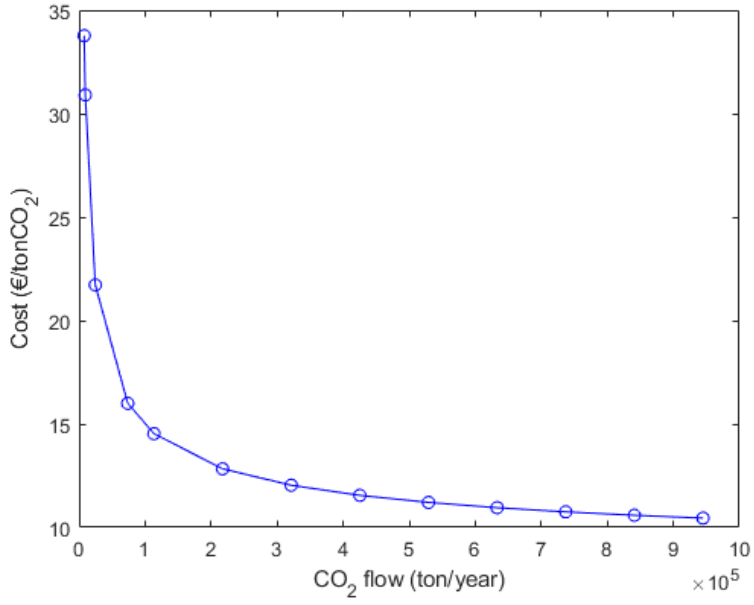

Figure 6.14: Effect on increasing the CO_2 flowrate for larger facilities

The design parameters for the base case were set to a liquefaction pressure of 27.5 bar according to the cost optimum case by Deng et al. [2]. Modifying this variable affects both compressor work and liquefier duty. A higher liquefaction pressure results in evidently higher CO_2 compression train work, but also decreases the liquefier duty. Decreasing the liquefier duty in turn decreases the compression power of the

refrigeration cycle, which is the biggest compressor. A third variable affected is the water removed in the CO_2 compression train. Higher liquefaction pressures should result in more water condensation in the intercoolers of the compression train. Figure 6.15 shows the clear effect that liquefaction pressure has on liquefier duty (top left), compression work for the three compressor stages (top right), and water content of the CO_2 when entering the dehydration unit.

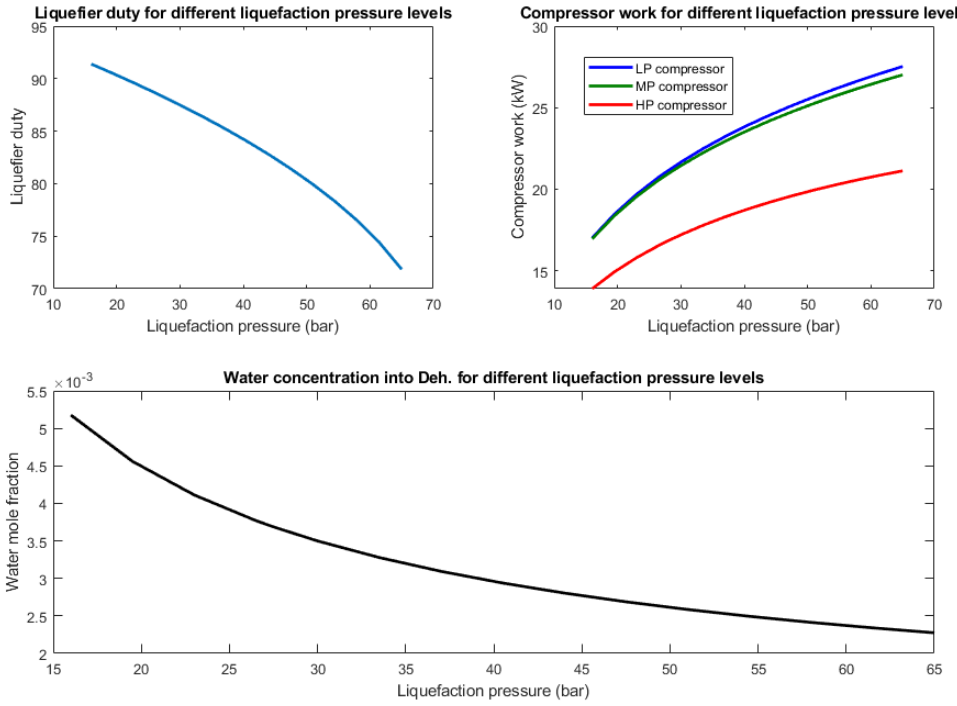

Figure 6.15: Effect of liquefaction pressure on liquefier duty, compressor work, and concentration of water into the dehydrator. The top left graph shows the liquefier cooling duty, the top right graph shows the compressor work of the three compressors in the CO_2 compression train, and the graph below shows the water content of the CO_2 flow coming into the dehydrator

The results are as expected. However, the difference in water removal before the dehydrator when increasing the pressure up to 65 bar is small and considered negligible. Moreover, the dehydrator costs are too small to consider a relevant effect of removing more water before dehydration. Nonetheless, increasing the liquefaction pressure has the opposite effect on the work required by the CO_2 compression train and the NH_3 cycle compressor. The effect of liquefaction pressure on total specific costs for CO_2 liquefaction is shown in Figure 6.16.

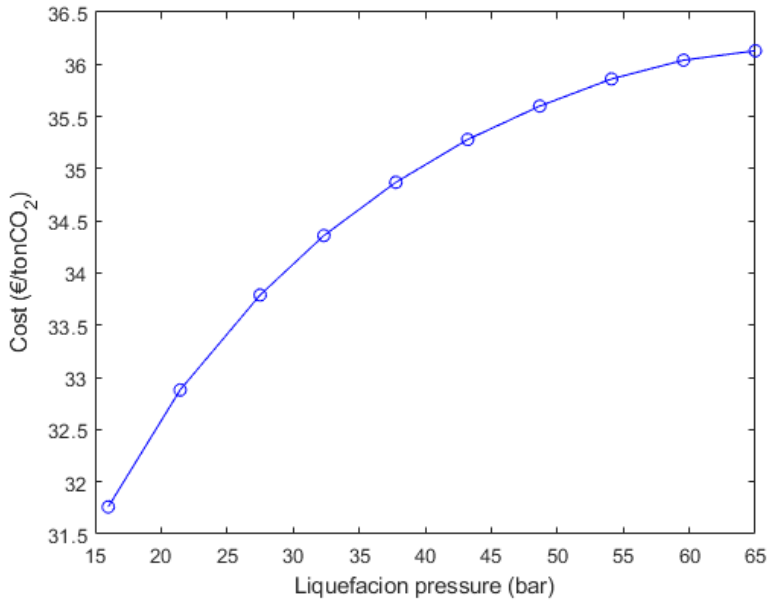

Figure 6.16: Effect of liquefaction pressure on total specific CO_2 liquefaction cost

Contrary to the results from Deng et al. [2], the lowest specific liquefaction cost is found at the lowest liquefaction pressure level possible, which is equal to the delivery pressure of 16 bar. This is because the reduction in compression work for the NH_3 cycle at higher liquefaction pressure is not as significant as the increase in the CO_2 compression train work, as it is shown in Figure 6.17. Thus, there is an overall increase in compression work required, which is reflected in higher CAPEX for larger compressors and higher OPEX for higher electricity consumption. In conclusion, although this study considers a liquefaction pressure of 27.5 bar, a pressure of 16 bar (or slightly higher to account for pressure losses not considered in the models) would be advisable. Consequently, there would be no need for CO_2 expansion to the delivery pressure, since the liquefaction pressure would be the same. Nonetheless, this conclusion applies only to pure CO_2 and the effect of impurities might present a different tendency.

According to the findings by Deng et al. [2], when the liquefaction pressure is low, there is a reduction in the total compression work as the pressure is increased, reaching a minimum at the optimal liquefaction pressure of 27.5 bar for a pure CO2 feed. From this point, the authors report an increase in total compression work that is mainly caused by the increase in work from the re-compressor (RC). In this study, RC remains un-activated, still resulting in an increase in total compression work at higher liquefaction pressure, as can be seen in Figure 6.17.

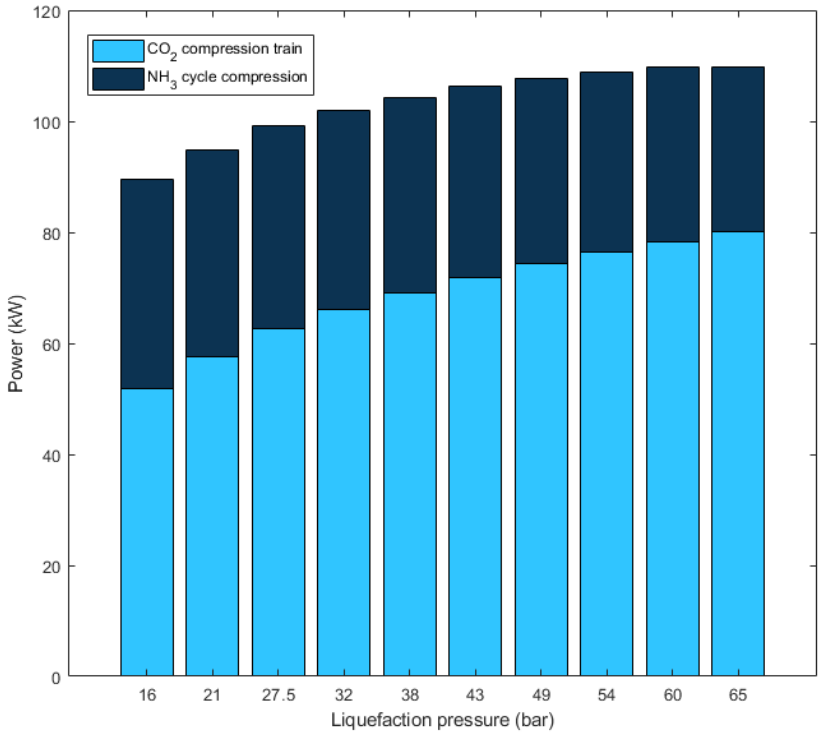

Figure 6.17: Effect of liquefaction pressure on compression work for the CO_2 compression train and the NH_3 refrigeration cycle

6.2.3.1 Future electricity market price projection sensitivity

This section intends to present an additional sensitivity analysis based on how future electricity prices could affect the costs of liquefaction. By varying the electricity price from a low value of 20 €/MWh to 100 €/MWh, Figure 6.18 was reproduced for three different interest rates.

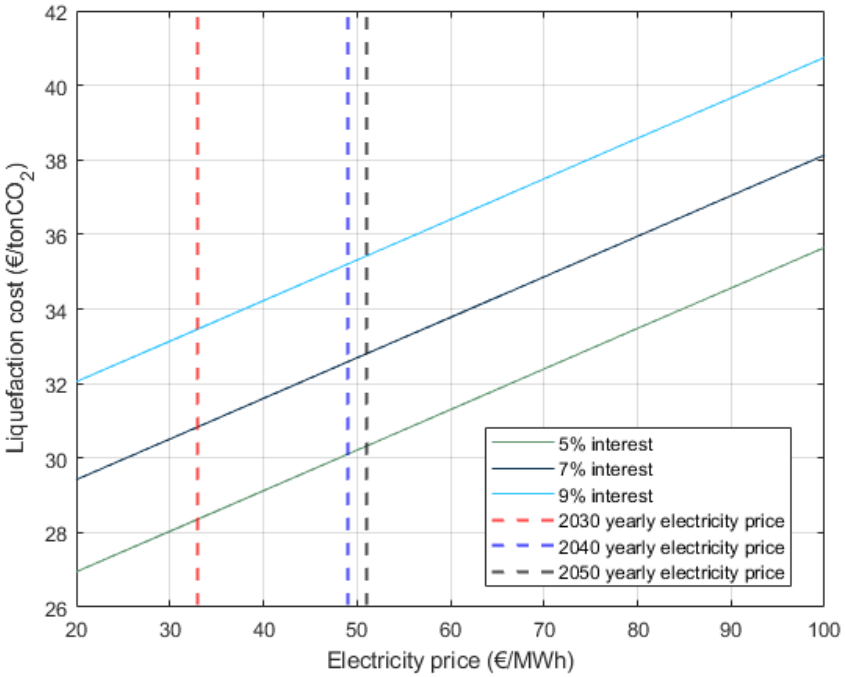

Figure 6.18: Effect of different electricity prices on liquefaction cost for different interest rate cases. Vertical dashed lines show the projected annual mean electricity prices for Southern Sweden in 2030, 2040, and 2050.

The interest rate used changes the liquefaction cost by just 2 €/tonCO_2, which is not considerable. With a very high electricity price of 100 €/MWh, the liquefaction cost for an interest rate of 7% would be close to 38 €/tonCO_2, in contrast with close to 30 €/tonCO_2 for a price of 20 €/MWh. It is anticipated that electricity prices will undergo significant fluctuations in the coming years due to the growing proportion of renewable energy sources and the associated variability they bring. In contrast to e-MeOH synthesis, the impact of electricity prices on liquefaction costs is relatively insignificant.

7
Conclusion

Biogenic CO_2 has the potential to be sold to different industries, with the intent to make products and processes net-zero or, in some cases, net-negative. In this scenario, liquefaction of CO_2 is necessary before transportation, unless it is sold to an industry located in close proximity to the source. Incorporating a liquefaction plant into Gasendal wouldn't be feasible when compared to other larger CO_2 emitters. Furthermore, negative emission incentives would be focused on the largest emitters with lower costs. CO_2 liquefaction for Gasendal would cost approximately 34 €/tonCO_2 when the lowest liquefaction costs could potentially reach 10 €/tonCO_2.

On the other hand, integrating a utilization plant to produce e-MeOH to Gasendal could only be beneficial if the price for the produced e-MeOH is at least two times higher than the one considered in this project of 0.495 €/tonMeOH. Moreover, it seems beneficial to purchase green hydrogen from the market, rather than producing it on-site, given that H_2 synthesis accounts for over 90% of the e-MeOH production costs. Comparing the feasibility of both options (i.e. liquefaction and e-MeOH synthesis) without knowing the actual incentives that could be given to implementing the processes is complicated, but setting up a utilization plant would appear to be an excellent pilot project.

The CO_2 liquefaction plant only requires cooling, and recovering heat to be used for Gasendal is not a feasible option because only 19 kW can be recovered out of the 700 kW required. In terms of DH, 85 kW could be potentially utilized. This is a small amount considering that there is no close connection to the DH network. No further improvements can be implemented to the process as the plant is already designed for maximum cooling. Moreover, there are limited streams available at the specific temperature level of 110°C, which is necessary for Gasendal. Nonetheless, the e-MeOH process could potentially supply 43% of the required heat by the reboiler at Gasendal. Additionally, this amount could be increased by designing the CO_2 compression inter-cooling differently. That is if the inter-cooling temperature was set below 128°C. A cost optimization of this design could be made in future work to try to reduce Gasendal's natural gas consumption even more. The e-MeOH synthesis plant can recover almost all of its heat demand within the process with the exception of 22.93 kW.

Future electricity prices might be very variable with the incorporation of more renewables into the system. Therefore, it becomes hard to provide a trustworthy estimate on how the feasibility of these projects might change given future market

conditions. That is also because the method employed in this thesis was using a constant electricity price. It is expected, however, that yearly electricity prices will be lower than 66 €/MWh, which was used in this study. A sensitivity analysis on the effect of electricity prices was conducted, and it can be concluded that it has a small effect on the liquefaction process. However, the effect is more significant for the e-MeOH synthesis because of the high electricity consumption from water electrolysis. The cost of e-MeOH could go to about 0.8 €/kgMeOH, which would still be higher than the current methanol price, for an electricity price of 20 €/MWh (lower than the yearly average estimated for the following decades). The cost of e-MeOH is expected to exceed the current market price of fossil MeOH. It could be argued that a cost of 0.8 €/tonMeOH would be a feasible threshold for making this project economically viable at an electricity price level of 20 €/MWh. Furthermore, an e-MeOH market price of around 1 €/kgMeOH would be the break-even market price if green H_2 is bought at a price of 4 €/kg.

A sensitivity analysis was performed on the size of the plant. For liquefaction, the effects of increasing the amount of liquefied CO_2 are considerable. Increasing the flow to up to 1M tonCO_2/year would reduce liquefaction costs to close to 10 €/tonCO_2, making this process comparable to other studies. On the other hand, the e-MeOH synthesis shows no decrease in total costs when increasing the CO_2 inlet flow because in this project the electrolysis total cost stays constant. Integrating such processes into a biomass-powered CHP plant, for example, would present other challenges not addressed in this thesis. That is because the CO_2 captured could contain high levels of impurities that would need to be removed. Such impurities cannot be present in liquefied CO_2 to be sold or stored and can interfere with the catalyst in the utilization plant.

Bibliography

[1] "Global energy-related CO2 emissions by sector – Charts – Data & Statistics." [Online]. Available: https://www.iea.org/data-and-statistics/charts/global-energy-related-co2-emissions-by-sector

[2] H. Deng, S. Roussanaly, and G. Skaugen, "Techno-economic analyses of CO2 liquefaction: Impact of product pressure and impurities," *International Journal of Refrigeration*, vol. 103, pp. 301–315, Jul. 2019. [Online]. Available: https://www.sciencedirect.com/science/article/pii/S0140700719301677

[3] C. Hammar, "Heat integration between CO2 Capture and Liquefaction and a CHP Plant: Impact on Electricity and District Heating Delivery at Renova's CHP Plant in Sävenäs," Master's thesis, Chalmers University of Technology, Gothenburg, 2022. [Online]. Available: https://hdl.handle.net/20.500.12380/304511

[4] L. Göransson, M. Lehtveer, E. Nyholm, M. Taljegard, and V. Walter, "The Benefit of Collaboration in the North European Electricity System Transition—System and Sector Perspectives," *Energies*, vol. 12, no. 24, p. 4648, Jan. 2019, number: 24 Publisher: Multidisciplinary Digital Publishing Institute. [Online]. Available: https://www.mdpi.com/1996-1073/12/24/4648

[5] "Biogenic CO2 from the biogas industry | European Biogas Association." [Online]. Available: https://www.europeanbiogas.eu/biogenic-co2-from-the-biogas-industry/

[6] A. H. Reksten, M. S. Thomassen, S. Møller-Holst, and K. Sundseth, "Projecting the future cost of PEM and alkaline water electrolysers; a CAPEX model including electrolyser plant size and technology development," *International Journal of Hydrogen Energy*, vol. 47, no. 90, pp. 38 106–38 113, Nov. 2022. [Online]. Available: https://www.sciencedirect.com/science/article/pii/S0360319922040253

[7] "Miljörapport 2020 Arendal biogasanläggning (Gasendal)," Göteborg Energi AB, Tech. Rep., 2020. [Online]. Available: https://www.goteborgenergi.se/Files/Webb20/Kategoriserad%20information/Informationsmaterial/Milj%C3%B6rapporter/2020/MR%20Arendal%20biogasanl%C3%A4ggning%20(Gasendal)%202020.pdf?TS=637570014517050697

[8] G. Towler and R. Sinnott, "Chapter 6 - Costing and project evaluation," in *Chemical Engineering Design*, first edition ed., G. Towler and R. Sinnott, Eds. Butterworth-Heinemann, 2008, pp. 298–397.

[9] EIGA, "Carbon Dioxide Food and Beverages Grade, Source Qualification, Quality Standards and Verification," 2016, doc. 70/17.

[10] "Northern Lights – How to store CO2 with Northern Lights." [Online]. Available: https://norlights.com/how-to-store-co2-with-northern-lights/

[11] "Paris Agreement," 2015.

[12] "Surface air temperature for January 2023 | Copernicus," Jan. 2023. [Online]. Available: https://climate.copernicus.eu/surface-air-temperature-january-2023

[13] M. Lehtveer, S. Brynolf, and M. Grahn, "What Future for Electrofuels in Transport? Analysis of Cost Competitiveness in Global Climate Mitigation," *Environmental Science & Technology*, vol. 53, no. 3, pp. 1690–1697, 2019, _eprint: https://doi.org/10.1021/acs.est.8b05243. [Online]. Available: https://doi.org/10.1021/acs.est.8b05243

[14] E. Zinn and H. Thunman, "Göteborg Energi: Vehicle Fuel From Organic Waste," in *Industrial Biorenewables*. John Wiley & Sons, Ltd, 2016, pp. 255–265, section: 10 _eprint: https://onlinelibrary.wiley.com/doi/pdf/10.1002/9781118843796.ch10. [Online]. Available: https://onlinelibrary.wiley.com/doi/abs/10.1002/9781118843796.ch10

[15] J. Agersborg and E. Lingehed, "Integration of Power-to-Gas in Gasendal and GoBiGas," Master's thesis, Chalmers University of Technology, Gothenburg, 2013. [Online]. Available: https://hdl.handle.net/20.500.12380/182610

[16] R. o. Regeringskansliet, "Sweden's climate policy framework," Mar. 2021, publisher: Regeringen och Regeringskansliet. [Online]. Available: https://www.government.se/articles/2021/03/swedens-climate-policy-framework/

[17] J. F. D. Tapia, J.-Y. Lee, R. E. H. Ooi, D. C. Y. Foo, and R. R. Tan, "A review of optimization and decision-making models for the planning of CO2 capture, utilization and storage (CCUS) systems," *Sustainable Production and Consumption*, vol. 13, pp. 1–15, 2018. [Online]. Available: https://www.sciencedirect.com/science/article/pii/S2352550917300453

[18] N. Jain, A. Srivastava, and T. N. Singh, "Carbon Capture, Transport and Geologic Storage: A Brief Introduction," in *Geologic Carbon Sequestration: Understanding Reservoir Behavior*, V. Vishal and T. Singh, Eds. Cham: Springer International Publishing, 2016, pp. 3–18. [Online]. Available: https://doi.org/10.1007/978-3-319-27019-7_1

[19] M. Grahn, E. Malmgren, A. D. Korberg, M. Taljegard, J. E. Anderson, S. Brynolf, J. Hansson, I. R. Skov, and T. J. Wallington, "Review of electrofuel feasibility—cost and environmental impact," *Progress in Energy*, vol. 4, no. 3, p. 032010, Jun. 2022, publisher: IOP Publishing. [Online]. Available: https://dx.doi.org/10.1088/2516-1083/ac7937

[20] I. Ridjan, B. V. Mathiesen, and D. Connolly, "Terminology used for renewable liquid and gaseous fuels based on the conversion of electricity: a review," *Journal of Cleaner Production*, vol. 112, pp. 3709–3720, 2016. [Online]. Available: https://www.sciencedirect.com/science/article/pii/S0959652615006964

[21] K. Atsonios, K. D. Panopoulos, and E. Kakaras, "Investigation of technical and economic aspects for methanol production through CO2 hydrogenation," *International Journal of Hydrogen Energy*, vol. 41, no. 4, pp. 2202–2214,

2016. [Online]. Available: https://www.sciencedirect.com/science/article/pii/S0360319915302718

[22] D. S. Marlin, E. Sarron, and O. Sigurbjörnsson, "Process Advantages of Direct CO2 to Methanol Synthesis," *Frontiers in Chemistry*, vol. 6, 2018. [Online]. Available: https://www.frontiersin.org/articles/10.3389/fchem.2018.00446

[23] F. Dalena, A. Senatore, A. Marino, A. Gordano, M. Basile, and A. Basile, "Chapter 1 - Methanol Production and Applications: An Overview," in *Methanol*, A. Basile and F. Dalena, Eds. Elsevier, 2018, pp. 3–28. [Online]. Available: https://www.sciencedirect.com/science/article/pii/B9780444639035000017

[24] M. Bowker, "Methanol Synthesis from CO2 Hydrogenation," *ChemCatChem*, vol. 11, no. 17, pp. 4238–4246, 2019, _eprint: https://chemistry-europe.onlinelibrary.wiley.com/doi/pdf/10.1002/cctc.201900401. [Online]. Available: https://chemistry-europe.onlinelibrary.wiley.com/doi/abs/10.1002/cctc.201900401

[25] A. Rufer, "Quantitative Design of a New e-Methanol Production Process," *Energies*, vol. 15, no. 24, 2022. [Online]. Available: https://www.mdpi.com/1996-1073/15/24/9309

[26] P. Borisut and A. Nuchitprasittichai, "Methanol Production via CO2 Hydrogenation: Sensitivity Analysis and Simulation—Based Optimization," *Frontiers in Energy Research*, vol. 7, 2019. [Online]. Available: https://www.frontiersin.org/article/10.3389/fenrg.2019.00081

[27] R. Pinsky, P. Sabharwall, J. Hartvigsen, and J. O'Brien, "Comparative review of hydrogen production technologies for nuclear hybrid energy systems," *Progress in Nuclear Energy*, vol. 123, p. 103317, May 2020. [Online]. Available: https://www.sciencedirect.com/science/article/pii/S014919702030069X

[28] S. Shiva Kumar and H. Lim, "An overview of water electrolysis technologies for green hydrogen production," *Energy Reports*, vol. 8, pp. 13 793–13 813, Nov. 2022. [Online]. Available: https://www.sciencedirect.com/science/article/pii/S2352484722020625

[29] J. Li, W. Liu, and W. Qi, "Hydrogen production technology by electrolysis of water and its application in renewable energy consumption," *E3S Web of Conferences*, vol. 236, p. 02001, 2021, publisher: EDP Sciences. [Online]. Available: https://www.e3s-conferences.org/articles/e3sconf/abs/2021/12/e3sconf_icersd2020_02001/e3sconf_icersd2020_02001.html

[30] S. Krishnan, M. Fairlie, P. Andres, T. de Groot, and G. Jan Kramer, "Chapter 10 - Power to gas (H2): alkaline electrolysis," in *Technological Learning in the Transition to a Low-Carbon Energy System*, M. Junginger and A. Louwen, Eds. Academic Press, Jan. 2020, pp. 165–187. [Online]. Available: https://www.sciencedirect.com/science/article/pii/B9780128187623000108

[31] A. B. T. Nelabhotla, D. Pant, and C. Dinamarca, "Chapter 8 - Power-to-gas for methanation," in *Emerging Technologies and Biological Systems for Biogas Upgrading*, N. Aryal, L. D. Mørck Ottosen, M. V. Wegener Kofoed, and D. Pant, Eds. Academic Press, Jan. 2021, pp. 187–221. [Online]. Available: https://www.sciencedirect.com/science/article/pii/B9780128228081000088

[32] M. Pérez-Fortes, J. C. Schöneberger, A. Boulamanti, and E. Tzimas, "Methanol synthesis using captured CO2 as raw material: Techno-economic and environmental assessment," *Applied Energy*, vol. 161, pp. 718–732, 2016. [Online]. Available: https://www.sciencedirect.com/science/article/pii/S0306261915009071

[33] G. H. Graaf, P. J. J. M. Sijtsema, E. J. Stamhuis, and G. E. H. Joosten, "Chemical equilibria in methanol synthesis," *Chemical Engineering Science*, vol. 41, no. 11, pp. 2883–2890, Jan. 1986. [Online]. Available: https://www.sciencedirect.com/science/article/pii/0009250986800197

[34] G. H. Graaf, E. J. Stamhuis, and A. A. C. M. Beenackers, "Kinetics of low-pressure methanol synthesis," *Chemical Engineering Science*, vol. 43, no. 12, pp. 3185–3195, Jan. 1988. [Online]. Available: https://www.sciencedirect.com/science/article/pii/0009250988851273

[35] G. H. Graaf, H. Scholtens, E. J. Stamhuis, and A. A. C. M. Beenackers, "Intra-particle diffusion limitations in low-pressure methanol synthesis," *Chemical Engineering Science*, vol. 45, no. 4, pp. 773–783, Jan. 1990. [Online]. Available: https://www.sciencedirect.com/science/article/pii/000925099085001T

[36] C. Seidel, A. Jörke, B. Vollbrecht, A. Seidel-Morgenstern, and A. Kienle, "Kinetic modeling of methanol synthesis from renewable resources," *Chemical Engineering Science*, vol. 175, pp. 130–138, Jan. 2018. [Online]. Available: https://www.sciencedirect.com/science/article/pii/S0009250917305973

[37] M. F. Torcida, D. Curto, and M. Martín, "Design and optimization of CO2 hydrogenation multibed reactors," *Chemical Engineering Research and Design*, vol. 181, pp. 89–100, 2022. [Online]. Available: https://www.sciencedirect.com/science/article/pii/S0263876222001058

[38] C. Becker, "From Langmuir to Ertl: The "Nobel" History of the Surface Science Approach to Heterogeneous Catalysis," in *Encyclopedia of Interfacial Chemistry*, K. Wandelt, Ed. Oxford: Elsevier, Jan. 2018, pp. 99–106. [Online]. Available: https://www.sciencedirect.com/science/article/pii/B9780124095472135279

[39] A. Aspelund, M. J. Mølnvik, and G. De Koeijer, "Ship Transport of CO2: Technical Solutions and Analysis of Costs, Energy Utilization, Exergy Efficiency and CO2 Emissions," *Chemical Engineering Research and Design*, vol. 84, no. 9, pp. 847–855, Sep. 2006. [Online]. Available: https://www.sciencedirect.com/science/article/pii/S0263876206729665

[40] W. Gong, E. Remiezowicz, P. L. Fosbøl, and N. von Solms, "Design and Analysis of Novel CO2 Conditioning Process in Ship-Based CCS," *Energies*, vol. 15, no. 16, p. 5928, Jan. 2022, number: 16 Publisher: Multidisciplinary Digital Publishing Institute. [Online]. Available: https://www.mdpi.com/1996-1073/15/16/5928

[41] "CO2LOS - CO2 ship transport - new solutions," Sep. 2019. [Online]. Available: https://www.sintef.no/en/projects/2019/co2los-co2-ship-transport-new-solutions/

[42] "CO2LOS II - Final Report with toolbox for CCS logistics," SINTEF, Tech. Rep. 19204-Z-RA-100-001, Dec. 2020. [Online]. Available: https://www.sintef.no/en/projects/2019/co2los-co2-ship-transport-new-solutions/report/

[43] "CinfraCap – Gemensam infrastruktur för transport av koldioxid, Förstudierapport," Mar. 2021. [Online]. Available: https://www.goteborgshamn.se/globalassets/cinfracap-forstudie-23-april-2021.pdf

[44] M. Ram, A. Aghahosseini, and C. Breyer, "Job creation during the global energy transition towards 100% renewable power system by 2050," *Technological Forecasting and Social Change*, vol. 151, p. 119682, 2020. [Online]. Available: https://www.sciencedirect.com/science/article/pii/S0040162518314112

[45] N. Meunier, R. Chauvy, S. Mouhoubi, D. Thomas, and G. D. Weireld, "Alternative production of methanol from industrial CO2," *Renewable Energy*, vol. 146, pp. 1192–1203, 2020. [Online]. Available: https://www.sciencedirect.com/science/article/pii/S0960148119310304

[46] A. K. Coker, "Chapter 18 - Compression Equipment (Including Fans)," in *Ludwig's Applied Process Design for Chemical and Petrochemical Plants (Fourth Edition)*, A. K. Coker, Ed. Boston: Gulf Professional Publishing, Jan. 2015, pp. 729–978. [Online]. Available: https://www.sciencedirect.com/science/article/pii/B9780080942421000188

[47] J. Kemper, L. Sutherland, J. Watt, and S. Santos, "Evaluation and Analysis of the Performance of Dehydration Units for CO2 Capture," *Energy Procedia*, vol. 63, pp. 7568–7584, Jan. 2014. [Online]. Available: https://www.sciencedirect.com/science/article/pii/S1876610214026071

[48] G. Cinti, R. Anantharaman, E. De Lena, C. Fu, S. O. Gardarsdottir, H. Hoppe, A. Jamali, M. Romano, S. Roussanaly, M. Spinelli, O. Stallmann, and M. Voldsund, "D4.4 Cost of critical components in CO2 capture processes," Oct. 2018. [Online]. Available: https://www.zenodo.org/record/2593219

[49] "CEMCAP." [Online]. Available: https://www.sintef.no/projectweb/cemcap/

[50] A. Francis, R. M.S, S. S. Priya, S. H. Kumar, K. Sudhakar, W. K. Fan, and M. Tahir, "Carbon dioxide hydrogenation to methanol: Process simulation and optimization studies," *International Journal of Hydrogen Energy*, vol. 47, no. 86, pp. 36 418–36 432, 2022. [Online]. Available: https://www.sciencedirect.com/science/article/pii/S0360319922038253

[51] X. Zhen, "Chapter 11 - Methanol As An Internal Combustion on Engine Fuel," in *Methanol*, A. Basile and F. Dalena, Eds. Elsevier, Jan. 2018, pp. 313–337. [Online]. Available: https://www.sciencedirect.com/science/article/pii/B978044463903500011X

[52] W. L. Luyben, "Estimating refrigeration costs at cryogenic temperatures," *Computers & Chemical Engineering*, vol. 103, pp. 144–150, Aug. 2017. [Online]. Available: https://www.sciencedirect.com/science/article/pii/S0098135417301394

[53] T. Berntsson, S. Harvey, and M. Morandin, "5 - Application of Process Integration to the Synthesis of Heat and Power Utility Systems Including Combined Heat and Power (CHP) and Industrial Heat Pumps," in *Handbook of Process Integration (PI)*, ser. Woodhead Publishing Series in Energy, J. J. Klemeš, Ed. Woodhead Publishing, Jan. 2013, pp. 168–200. [Online]. Available: https://www.sciencedirect.com/science/article/pii/B9780857095930500058

[54] P. Thollander, M. Karlsson, P. Rohdin, J. Wollin, and J. Rosenqvist, "13 - Energy management," in *Introduction to Industrial Energy Efficiency*,

P. Thollander, M. Karlsson, P. Rohdin, J. Wollin, and J. Rosenqvist, Eds. Academic Press, Jan. 2020, pp. 239–257. [Online]. Available: https://www.sciencedirect.com/science/article/pii/B9780128172476000134

[55] G. Towler and R. Sinnott, "Chapter 13 - Mechanical design of process equipment," in *Chemical Engineering Design*, first edition ed., G. Towler and R. Sinnott, Eds. Butterworth-Heinemann, 2008, pp. 961–1063.

[56] "Cost Indices – Towering Skills." [Online]. Available: https://toweringskills.com/financial-analysis/cost-indices/

[57] "Day.ahead prices." [Online]. Available: https://www.nordpoolgroup.com/en/Market-data1/Dayahead/Area-Prices/ALL1/Hourly/

[58] B. Lacerda de Oliveira Campos, K. John, P. Beeskow, K. Herrera Delgado, S. Pitter, N. Dahmen, and J. Sauer, "A Detailed Process and Techno-Economic Analysis of Methanol Synthesis from H2 and CO2 with Intermediate Condensation Steps," *Processes*, vol. 10, no. 8, p. 1535, Aug. 2022, number: 8 Publisher: Multidisciplinary Digital Publishing Institute. [Online]. Available: https://www.mdpi.com/2227-9717/10/8/1535

[59] W. Kuckshinrichs, T. Ketelaer, and J. C. Koj, "Economic Analysis of Improved Alkaline Water Electrolysis," *Frontiers in Energy Research*, vol. 5, 2017. [Online]. Available: https://www.frontiersin.org/articles/10.3389/fenrg.2017.00001

[60] S. Brynolf, M. Taljegard, M. Grahn, and J. Hansson, "Electrofuels for the transport sector: A review of production costs," *Renewable and Sustainable Energy Reviews*, vol. 81, Jun. 2017.

[61] F. Chen and T. Morosuk, "Exergetic and Economic Evaluation of CO2 Liquefaction Processes," *Energies*, vol. 14, no. 21, p. 7174, Jan. 2021, number: 21 Publisher: Multidisciplinary Digital Publishing Institute. [Online]. Available: https://www.mdpi.com/1996-1073/14/21/7174

[62] L. E. Øi, N. Eldrup, U. Adhikari, M. H. Bentsen, J. L. Badalge, and S. Yang, "Simulation and Cost Comparison of CO2 Liquefaction," *Energy Procedia*, vol. 86, pp. 500–510, Jan. 2016. [Online]. Available: https://www.sciencedirect.com/science/article/pii/S1876610216000539

[63] J. Cortés Romea, "Electrified District Heating Plants using Thermochemical Energy Storage," Master's thesis, Chalmers University of Technology, Gothenburg, 2023. [Online]. Available: http://hdl.handle.net/20.500.12380/306022

[64] "Commission Regulation (EU) No 231/2012 of 9 March 2012 laying down specifications for food additives listed in Annexes II and III to Regulation (EC) No 1333/2008 of the European Parliament and of the Council Text with EEA relevance," Mar. 2012, legislative Body: COM. [Online]. Available: http://data.europa.eu/eli/reg/2012/231/oj/eng

[65] S. Karlsson, F. Normann, M. Odenberger, and F. Johnsson, "Modeling the development of a carbon capture and transportation infrastructure for Swedish industry," *International Journal of Greenhouse Gas Control*, vol. 124, p. 103840, Mar. 2023. [Online]. Available: https://www.sciencedirect.com/science/article/pii/S1750583623000105

A

Appendix 1

Table A.1: Minimum pressure vessel thickness

Diameter (m)	Minimum thickness (mm)
1	5
1-2	7
2-2.5	9
2.5-3	10
3-3.5	12

A.1 Molecular sieve sizing and cost estimation

Based on [48] the following methodology is used to estimate the cost of a molecular sieve for CO_2 dehydration. Using an adsorbent cost of 3600 e $_2$015/ton, the direct cost for the molecular sieve (DC_{sieve}) is represented as follows,

$$DC_{sieve} = DC_{containers} + 3600e\,_2015/tonm_{adsorbent} \tag{A.1}$$

Where $DC_{containers}$ is the direct cost of the columns (i.e. adsorption and desorption) and $m_{adsorbent}$ is the mass of the adsorbent in tons. The following 6 steps are followed to size the dehydration unit.

Step 1: election of adsorbent.

Following the CEMCAP report a molecular sieve capacity of 16.8 kg of water per 100 kg of adsorbent is assumed. The adsorbent material has a bulk density of 720 kg/m^3.

Step 2 and 3: Given a pressure drop limit, superficial gas velocity, and bed cross-sectional area calculation.

The pressure drop per unit of length is determined as:

$$\Delta P/L = B\mu V + CdV^2 \tag{A.2}$$

Where, ΔP is the pressure drop through the bed (psi), L is the bed length (ft), μ is the gas viscosity (cp), V corresponds to superficial gas velocity (ft/min) and d is the density of the gas (lb/ft^3. $\Delta P/L$ can be assumed to be 0.33 psi/ft. B and C are

constants that depend on the geometry of the bed particles and the corresponding values are presented in

Table A.2: Constants A and B for different particle sizes and geometry

Particle type	B	C
1/8 in bead	0.0560	0.0000869
1/8 in extrudate	0.0722	0.000124
1/16 in bead	0.152	0.000136
1/16 in extrudate	0.238	0.00210

After finding V from Equation A.2, the cross-sectional area can be found.

$$A = \dot{V}/V \tag{A.3}$$

Where, A is the cross-sectional area (ft^2) and $\dot{V}$ is the volumetric gas flow rate (ft^3/min) extracted from the Aspen simulation results.

Step 4: finding the total length of the bed

The length of the bed is defined as the sum of the length of the equilibrium section (LES) plus the length of the unused bed (LUB)

$$LES = \frac{100G}{\rho_b}\frac{\Delta Y}{\Delta X}t \tag{A.4}$$

Where G is the gas inlet flow rate (kmol/hrm^2) obtained with the simulation's flow rate and the cross-sectional area, ρ_b is the bulk density of the adsorbent, ΔY is the water molar concentration in the gas inlet minus the concentration in equilibrium, ΔX is the adsorbent's design capacity (mole/100kg), and t is the time of adsorption (hr) which is usually 4 hours.

$$LUB = 1/2MTZ \tag{A.5}$$

Where, MTZ is the mass transfer zone and is calculated with the superficial gas velocity in ft/min.

$$MTZ = \left(\frac{V}{35}\right)^{0.3} Z \tag{A.6}$$

Where, Z is a constant that is equal to 1.7 for a bed particle size of 1/8 in and 0.85 for 1/16 in size.

Step 5: calculating the adsorber height and direct cost for the molecular sieve

The column height is calculated accounting for an extra 2 meters for column internals. The column's thickness is calculated based on a pressure vessel as presented in Section 4.2.6, and the purchase cost, or direct cost of the column is estimated following the methodology presented in Section 4.3. The purchase cost for the column

is multiplied times two (adsorber and desorber) and that corresponds to the value for $DC_{containers}$. After this, the direct cost for the molecular sieve can be calculated with Equation A.1. All the costs were calculated for 2023 using the appropriate CEPCI values presented in Section 4.3.

A.2 Detailed equipment cost results

Table A.3: Detailed purchased and installed equipment cost for the liquefaction process

Component ID	Comment	Size (S)	Size units	Purchase cost	Installed cost
LPC	Low pressure	20.85	kW	41,982 €	216,291 €
MPC	Medium pressure	20.93	kW	42,047 €	216,628 €
HPC	High pressure	20.94	kW	42,053 €	216,659 €
IC1	Low pressure	0.63	m^2	1,814 €	9,346 €
IC2	Medium pressure	0.63	m^2	1,819 €	9,373 €
IC3	High pressure	0.66	m^2	1,869 €	9,627 €
F1	Pre-compression	420.28	kg	12,523 €	64,520 €
F2	Low pressure	420.28	kg	12,523 €	64,520 €
F3	Medium pressure	420.28	kg	12,523 €	64,520 €
F4	High pressure	1209.90	kg	24,157 €	124,459 €
F5	Purge impurities	NA	-	- €	- €
F6	Recycle gasses and separate liquified CO2	NA	-	- €	- €
LIQ	Liquefier with ammonia as a refriferant	3.81	m^2	7,146 €	36,814 €
P	Pre-cooler with cooling water	0	m^2	- €	- €
V	Expansion to delivery pressure	NA	-	- €	- €
RC	From F6 to high pressure before liquefaction unit	NA	-	- €	- €
M	To mix HP recycle with HP gas after compression train	NA	-	- €	- €
IR	Dehydration unit and other impurity removal	Sized separately	-	2,737 €	14,100 €
RefC	From the refrigeration cycle	36.51	kW	53,644 €	276,375 €
RefC	From the refrigeration cycle	17.29	m2	17,539 €	90,361 €

Table A.4: Detailed purchased and installed equipment cost for the e-methanol synthesis base case (i.e. no heat integration) without considering electrolysis for hydrogen production

Component	Description	Size	Size unit	Ce (2023) EUR	Installed cost
C-H2	Hydrogen compressor	58.46	kW	66,980 €	345,082 €
C-CO2-1	CO2 compression	20.96	kW	42,078 €	216,784 €
C-CO2-2	CO2 compression	27.16	kW	47,003 €	242,158 €
C-CO2-3	CO2 compression	27.83	kW	47,503 €	244,737 €
C-CO2-4	CO2 compression	27.16	kW	47,001 €	242,150 €
IC-CO2-1	Intercooler after compression-1	0	m^2	- €	- €
IC-CO2-2	Intercooler after compression-2	0.17	m^2	15,245 €	78,541 €
IC-CO2-3	Intercooler after compression-3	0.20	m^2	15,249 €	78,561 €
IC-CO2-4	Intercooler after compression-4	0	m^2	- €	- €
PH	Reaction pre-heater	3.03	m^2	15,628 €	80,518 €
AC	Reaction after-cooler	10.20	m^2	16,589 €	85,469 €
D-PH	Destillation pre-heater	15.17	m^2	17,255 €	88,896 €
F1	Before CO2 compression to remove liquid	420.28	kg	12,523 €	64,520 €
F2	Un-reacted gasses separation	3651.37	kg	47,440 €	244,412 €
DC	Distillation column	875.59	kg	19,789 €	101,955 €
Trays	Distillation trays (per tray) -cost is for all trays	0.46	m	3,618 €	18,639 €
R	Reactor	Estimated separately	-	217,459 €	1,120,346 €

DEPARTMENT OF MECHANICS AND MARITIME SCIENCE
CHALMERS UNIVERSITY OF TECHNOLOGY
Gothenburg, Sweden
www.chalmers.se

CHALMERS
UNIVERSITY OF TECHNOLOGY